Response to the Referee #1

Dear Referee,

Thank you for the time that you spent on our manuscript. Below you will find a summary of the changes that we made throughout the manuscript to address all your suggestions.

Yours sincerely

On behalf of all the co-authors,

Guillian Van Achter

General comments

This study used a high-resolution (2km) regional ocean-sea ice-ice shelf model to investigate the responses of landfast ice, sea ice, ice-shelf basal melt, and ocean around the Totten Ice Shelf (TIS) to a future warming climate scenario (SSP4-4.5). The novelty of this study is applying the prognostic fast ice component that the authors developed as a part of a sea-ice model component in their previous study. Although I have several concerns and suggestions, I think that this paper will be suitable for publishing in The Cryosphere after substantial revision.

Specific comments

1. [Major] L9-11 "The representation of fast ice ..."and discussions with Table 2. This study concludes that the response of ice-shelf basal melting at the Totten Glacier becomes prominent in the experiments with landfast ice, compared to those without landfast ice. I think that the conclusion is slightly misleading. The areal extent of fast ice becomes small under the future warming condition, and there are no significant differences in the Totten Glacier melting between the numerical experiments with and without fast ice. A large difference in the TIS basal melting is only found in the present-day (1995-2014) condition, creating the tendency in the experiments with and without fast ice.

We changed the abstract, the results section and the conclusion to avoid further confusion. As you have summarised, there are no significant effect of the fast ice on the basal melt rate in the end of the 21st century. The effect of fast ice on the melt rate is important in the last decades simulation but then becomes negligible with the decrease of sea ice cover during the 21st century (see page 1 lines 12-13, pages 15-16 lines 238-240, page 17-18 lines 276-287).

2. [Major] The literature, Pelle et al. (2021), used a high emission scenario, but this study used the moderate one, SSP4-4.5, without any explanation/motivation. If possible, I strongly recommend performing additional experiments under high emission scenarios to compare the previous study and obtain more solid results under warming climates.

We acknowledge that the use of several emission scenarios would have be interesting. Nevertheless, as the moderate SSP4-4.5 scenario already sufficiently decreases the sea ice concentration to such an extent that the fast ice effect is not significant by the end of the 21st century, the use of a stronger emission scenario does not seem opportune to us to study the fast ice effect of the basal melt rate increase.

3. [Major] Which forcing drives the future changes in fast ice, sea ice, and ocean fields, atmospheric forcing or ocean forcing? Additional experiments to separate the effects and analyses on them are helpful for readers.

As suggested, we ran a new sets of simulations. WARM_noWind, is the same simulation as WARM but without the EC-Earth wind velocity anomalies over the atmospheric boundary conditions. WARM_noAtm, is the same simulation as WARM but without any EC-Earth3 anomaly on the atmospheric forcings. WARM_noOce, which is identical to WARM except that there are no EC-Earth3 anomaly on the ocean velocity forcing. These simulations aim to separate the ocean and the atmospheric forcing effects on the model.

As presented in Figure 1a, the EC-Earth anomaly applied at the atmospheric boundary have no effect on the ocean circulation. Indeed, WARM, WARM_noAtm and WARM_noWind have the same westward ocean transport. On the other hand, WARM_noOce shows a decreased Antarctic Slope Current (ASC) compared to WARM, which suggests that part (83%) of the intensification of the ASC in WARM compared to REF is due to the ocean velocity EC-Earth anomaly applied on the ocean boundary conditions. As the remaining part (13%) of the ASC intensification between REF and WARM is not related to the EC-Earth anomaly applied at the atmosphere, it implies that it is due to the changes in seawater density over the continental shelf. The manuscript has been adapted, with this new results and analysis (see pages 10-11, lines 168-193).
We also separate the effect of atmospheric and oceanic forcing on the changes in both sea ice and fast ice. As shown by the Figure 1b-e, the sea ice shows a sensitivity to the atmospheric velocity forcings. Without the EC-Earth3 atmospheric forcing, the sea ice concentration is higher everywhere, with a sea ice front located further north. The same effect is seen for the fast ice, with a higher fast ice frequency over the mutliyear fast ice pack without the atmospheric forcing. The manuscript has been adapted, with this new results and anlysis (see page 8, lines 160-163 and Fig.A1).

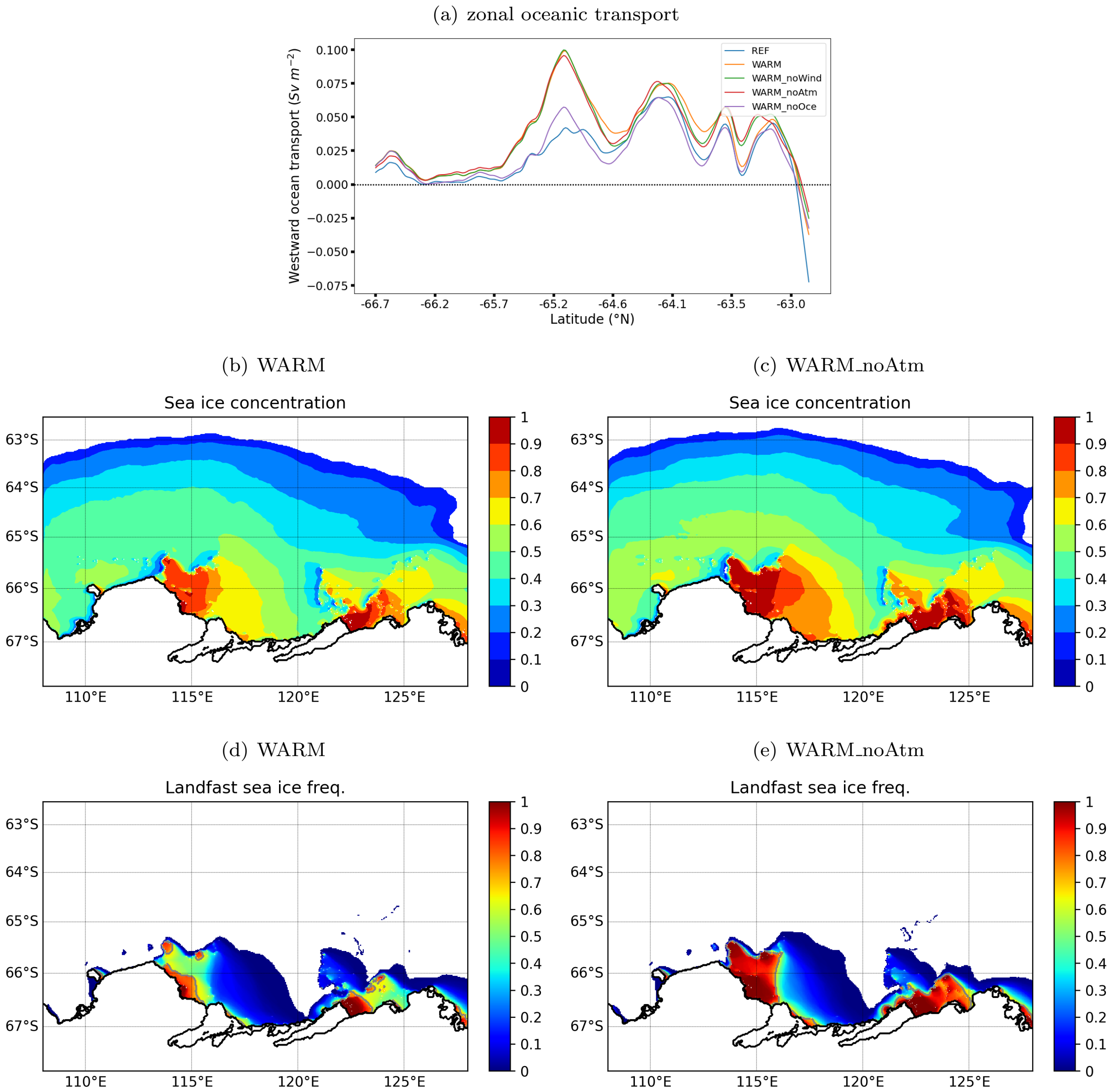

Figure 1: Differences in ocean transport, sea ice concentration and fast ice between the WARM and WARM_noAtm simulations.

4. [Major] L110-112 I don't think that the two-year spin-up is enough to obtain the quasi-steady states in oceanic variables. In fact, large declining trends in ice-shelf basal melting are found in the first seven years (Figs. 7 and 8). Are these model drift or interannual variability? To avoid including (or decreasing) the model drift signals, results from the second cycle (after the first cycle of the 20-year run) are preferable.

To address this question, we launched a new simulation, referred to as WARM_CI. This new simulation is the same as WARM except that it starts at the end of the WARM simulation (the equivalent of a 20yrs spin-up). As shown in Fig. 2, the ice shelf melt rates present the same drifted signals, which suggests that the drifted signal is independent of the initial conditions but is a direct consequence of the oceanic boundary conditions (here we only compare the first 10 years of simulations). The changes in basal melt rate due to the modifications of the ocean initial conditions are only observed during the first two years (more clearly in the Moscow University cavity) but then becomes negligible. All the simulations used in the manuscript have now a 20yrs spin-up (see page 5, line 134).

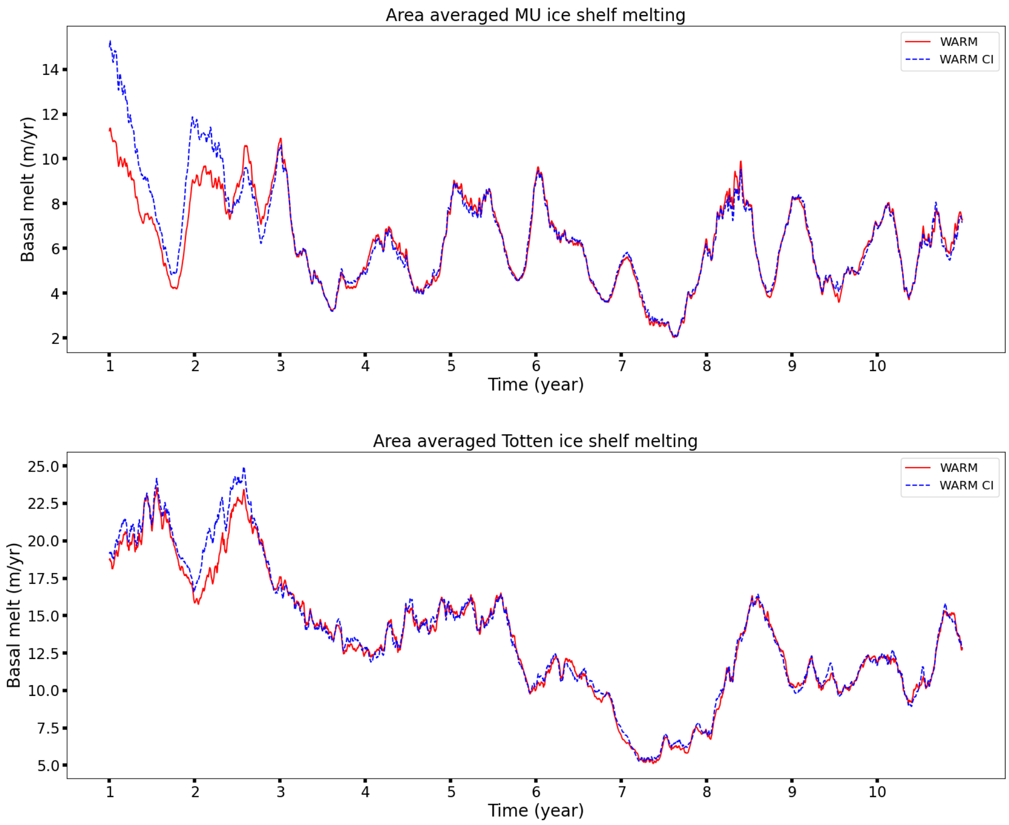

Figure 2: Ice shelves basal melt rate for the sensitivity experiments with a full spin-up of the model (in dashed blue) for both Moscow University (top) and Totten (bottom) ice shelves. The reference simulation (in red) is the simulation presented in the paper.

5. [Major] Pelle et al. (2021) pointed out that weakening of Antarctic Slope Front/Current is important for ice-ocean interaction in this region, but the lateral boundary condition in this study is the opposite (e.g., stronger slope current in the future). It is OK there are differences among the studies. This manuscript is a numerical modeling study, and thus I suggest that the author perform additional numerical experiments to identify the role of the strength of the slope current. It is also helpful to understand the difference between the studies.

Thanks to the WARM_noOce simulation, we can compare the effect of both a low and strong ASC intensity on the warm water exchanges across the shelf. The basal melt rate in both cavities for both the WARM and WARM_noOce simulations are presented in Figure 3. For both cavities, the simulation with the higher ASC intensity (WARM) has the lower basal melt rate. This result suggests that a stronger ASC decreases the warm water exchanges across the shelf and reduces the basal melt rate. These new results have been added to the manuscript (see page 11, lines 196-200).

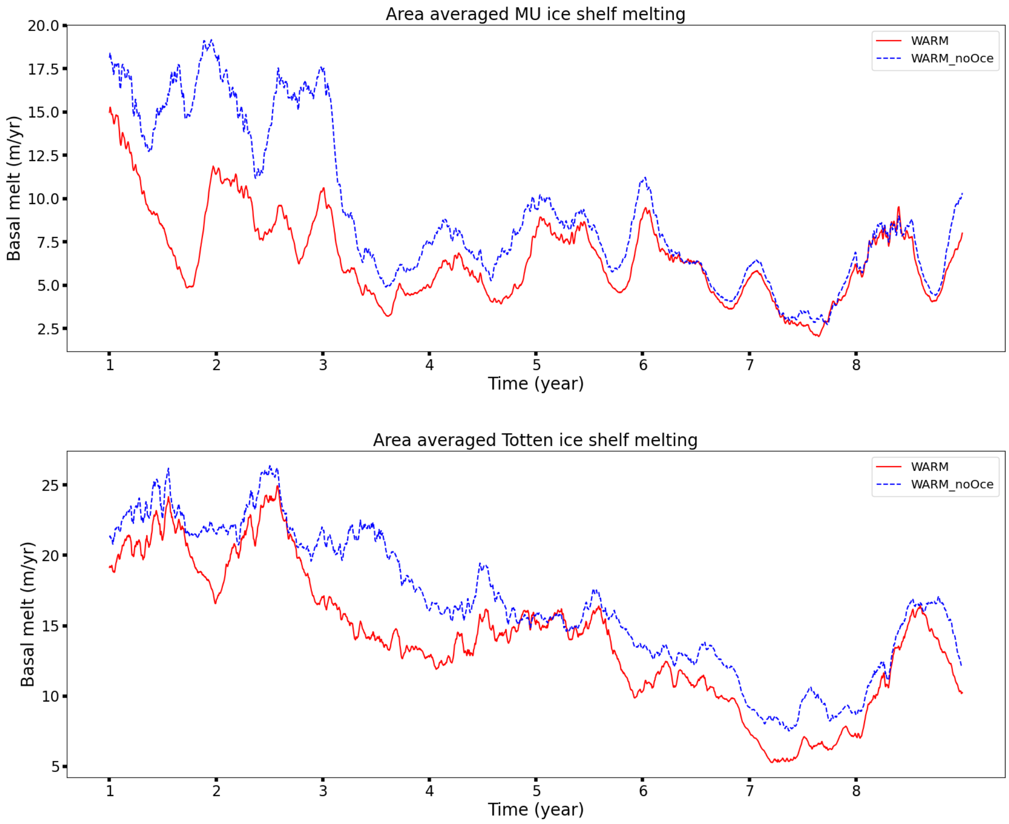

Figure 3: Ice shelves basal melt rate for the WARM and WARM_noOce simulations for both Moscow University (top) and Totten (bottom) ice shelves. The reference simulation (in red) is the simulation presented in the paper.

6. [Major] L155-156 "This acceleration mainly results from the retreat of fast ice, ...". No evidence in the manuscript supports this sentence.

This affirmation was made based on the mean barotropic ocean velocity changes between the REF and nFST simulations. The nFST simulation shows stronger ocean current near the coast compared to REF, especially where there are packs of fast ice. The manuscript has been updated (see page 10, lines 174-175, and Fig A2 in the manuscript).

7. [Major] L161-170. To examine the ASC intensification, some analyses of the climate model (EC-Earth3) on a wider scale are required. Since the ASC is a large-scale phenomenon, not only local wind but also wind over the remote Antarctic coastal regions becomes a driving force.

We updated the conclusion to emphasise that our results on the ASC are only valid over our local domain and that the winds, through their impact on the ocean circulation outside of the configuration have an impact on oceanic forcings applied over the configuration. An EC-Earth winds analysis outside of our region of interest is beyond the scope of this research paper. Furthermore, as described above, the analysis on the separate effect of atmospheric and oceanic forcings on the ocean circulation already provides additional information on that subject (see page 17, lines 196-198).

8. [Major] L197-199 and L226-228 There are no results on sea ice production in the manuscript.
As suggested, results of sea ice production have been added to the text (see pages 9-10, lines 165-169, and figure 5).

9. [Major] I think spatial distributions related to the ice shelf/glacier basal melt rate are missing in the manuscript.
Results about the spatial distribution of the basal melt rate have been added to the manuscript (see figure 8c).

Technical corrections

10. Figure2: Where are the locations of these observations? There are unrealistic connections in the profiles (probably connecting lines between different locations?).
The observations have been collected in two locations, in front of the Totten ice shelf cavity (these are the deeper profiles) and close to the Dalton coastal polynya (shallower profiles). The locations are now displayed in a new subfigure (see figure 2b).

11. Figures 5, 6, and 9: Please increase latitudes' tick marks (e.g., adding 65S and 67S if they are in the range).
We added more latitudes on each figures of the manuscript when possible, with ticker lines.

12. Figure3: Please use a linear scale for the vertical scale. Line or shade showing bottom topography is required for panels a-c. A vertical line showing the model domain (63S) is also helpful.
We preferred to keep the scale as it was, for better consistency with the other figures. Furthermore, since the ocean reaches more than 5000 meter depth outside the continental shelf, such a scale is useful to represent the ocean vertical profiles outside of the shelf. It keeps a large portion of the figure for the first hundred meters where most of the heterogeneity are and the rest of the figure is for the deep ocean where the ocean variables are often homogeneously distributed. Furthermore, we cut the figure at the correct domain size (the maximum latitude is now 63S). Showing the EC-Earth3 anomalies in the north of our domain was not relevant.

13. Figure 4: Please consider adding 0.75 contours in panels a-b to allow readers to compare the observational result (Fig. 1).
Done.

14. Figure 6: Please consider adding contours of the bottom topography.
Done.

15. Figures 7 and 8: Please use the same vertical scales, at least for the same regions (TIS for panel a and MUIS for panel b).
It has been done.

16. L268-269: References are required.
Done.

Influence of fast ice on future ice shelf melting in the Totten Glacier area, East Antarctica

Guillian Van Achter[1], Thierry Fichefet[1], Hugues Goosse[1], and Eduardo Moreno-Chamarro[2]

[1]Earth and Life Institute, Georges Lemaitre Centre for Earth and Climate Research, UCLouvain, Louvain-la-Neuve, Belgium.
[2]Barcelona Supercomputing Center (BSC), Barcelona, 08034, Spain.

Correspondence: Guillian Van Achter (guillian.vanachter@uclouvain.be)

Abstract. The Totten Glacier in East Antarctica is of major climatic interest because of the large fluctuations of its grounding line and potential vulnerability to climate change. Here, we use a series of high-resolution, regional NEMO-LIM-based experiments, which include an explicit treatment of ocean–ice shelf interactions as well as a representation of grounded icebergs and fast ice, to investigate the changes in ocean–ice interactions in the Totten Glacier area between the last decades (1995-2014) and the end of the 21st century (2081-2100) under SSP4-4.5 climate change conditions. By the end of the 21st century, the wide areas of multiyear fast ice simulated in the recent past are replaced by small patches of first year fast ice along the coast, which decreases the total summer sea ice extent. The Antarctic Slope Current is accelerated by more than ~~90~~116% and the Totten ice shelf melt rate is increased by ~~41~~91% due to enhanced warm water intrusions into its cavity. The representation of fast ice dampens the ice shelf melt rate increase throughout the 21st century, as the Totten ice shelf melt rate increase reaches ~~58~~136% when fast ice is not taken into account. The Moscow University ice shelf melt rate increase is even more impacted by the representation of fast ice, with a ~~1~~36% melt rate increase with fast ice, compared to a ~~38~~75% increase without a fast ice representation. Fast ice enhances the ice shelves basal melt rate for the last decades but holds a limited effect by the end of the 21st century due to the strong sea ice loss. This highlights the importance of including representation of fast ice to simulate realistic ice shelf melt rate increase in East Antarctica under warming conditions.

1 Introduction

The Totten Glacier area, located on the Sabrina Coast in East Antarctica, underwent significant grounding-line fluctuations during the recent past. Driven by changes in the ocean (Aitken et al., 2016), these fluctuations are making the region potentially vulnerable to rapid ice sheet collapse (Roberts et al., 2011). There has been some indication of ice shelf thinning during the last decade (Khazendar et al., 2013), although it remains unclear whether this represents a long-term trend (Paolo et al., 2015). Furthermore, the Totten catchment, located in the Aurora Subglacial Basin of East Antarctica, contains 3.5-m sea level rise equivalent and is one of the few sectors of East Antarctica where changes in ice dynamics have been observed recently (Greenbaum et al., 2015). Understanding how changes in the ocean–ice interactions are interfering with the basal melt of the Antarctic ice shelves and how they will evolve in the future is crucial for projections of future sea level rise.

A key element of the ocean–ice interactions in the Totten Glacier area is the fast ice (Van Achter et al., 2022), defined as stationary sea ice which forms and remains attached to the shore or between grounded icebergs (WMO, 1970; Massom et al., 2001; Fraser et al., 2012). Numerous observations show the presence of ~~multiyear~~ both multiyear and seasonal fast ice in front of both the Totten and Moscow University ice shelves (Fraser et al., 2012, 2020). Van Achter et al. (2022) have clearly demonstrated with a numerical model (over the years 2001-2010) that the presence of fast ice in the Totten Glacier region impacts ~~both the location of coastal polynyas and the ocean mixed layer depth~~ the all ice–ocean system. Fast ice grows through the advection of sea ice which forms ice arches between icebergs or between icebergs and the coast. Once the sea ice is trapped by the ice arches, it thickens by snow accumulation. Once established, a thick multiyear fast ice pack along the coast ~~, in addition to favouring the~~ thermodynamically isolates the ocean from the atmosphere during the Summer. In the Winter, both yearly and multiyear fast ice relocate the coastal polynyas off shore, which decreases the sea ice production close to the coast. These effects combined increase the ocean stratification in front of the cavities and it favours the intrusion of modified Circumpolar Deep Water (mCDW) into the ice shelf cavities, with an enhanced or reduced ice shelf melting depending on the location. ~~The~~ Fast ice can also have a dynamical influence on the ice shelf, as the loss of buttressing from the break-up of seasonal fast ice increases the seasonality of the Totten ice shelf (TIS) basal melt rate close to the ice front (Greene et al., 2018).

Large density, temperature, salinity and sea level gradients are found across the Antarctic Slope Front (ASF; Whitworth et al., 1985; Jacobs, 1991), which separates the continental shelf from the open Southern Ocean. A strong pressure gradient is observed across the ASF, mainly caused by the strong easterly winds that drive a sea surface height gradient via Ekman drift (Mathiot et al., 2011), as well as a density gradient, which results from the differences in temperature and salinity of the water masses across the ASF. Additionally, the ASF manifests itself through strong isopycnal doming towards the continental shelf. These lateral gradients across the ASF contribute to establishing the geostrophically balanced, vertically sheared along-slope flows of the Antarctic Slope Current (ASC; Jacobs, 1991; Thompson et al., 2018). The ocean dynamics associated with the ASF and ASC govern along- and across-slope heat transport (Stewart et al., 2018), and act as a barrier to mixing between shelf and open-ocean waters (Thompson et al., 2018). Shifts in position of the ASF, or changes in the range of densities of waters that occupy the continental shelf, ~~will~~ therefore strongly influence the heat budget of the continental shelf (Thompson et al., 2018). Moorman et al. (2020) suggested that increasing glacial meltwater fluxes strengthens the lateral density gradient associated with the ASF, which reduces cross-slope water exchanges and isolates shelf waters from warm mCDW. Naughten et al. (2018) also found an intensified density gradient across the continental slope which reinforces the Antarctic Coastal Current. In the Totten Glacier region, the ASC modulates the heat intrusion towards the Totten Glacier (Nakayama et al., 2021).

As a consequence, understanding how the ASC will evolve in this region under future climate conditions is key to gain insights on changes in heat intrusion across the continental shelf break. The future changes in ice shelf melt rate under different Representative Concentration Pathway (RCP) scenarios have been studied with both global and regional models (Hellmer et al., 2012; Timmermann and Goeller, 2017). In the Totten Glacier area, Pelle et al. (2021) found that, by the end of the 21st century, the ASC might weaken by 37% compared to its present-day state and the Totten ice shelf melt rate might increase by 56%

following a high emission scenario. Those models include representations of ocean–ice shelf interactions, but none of them has an prognostic representation of the fast ice.

The present study follows on from Van Achter et al. (2022), which presented a prognostic fast ice representation and investigated the impact of fast ice on ocean–ice interactions over the last decade. The goal of the present study is twofold. ~~Firstly, we want to~~ As climate warming leads to a reduction of the sea ice cover in the Southern Ocean and hence most likely to a reduction in the stability and duration of the fast ice cover, we first evaluate how the ocean–ice shelf interactions in the Totten Glacier region will change in a warming climate, with a particular focus on the ASC changes and their origin. Secondly, as a reduction in fast ice changes the atmosphere-ocean energy fluxes and impacts both the near-surface ocean currents and the ocean stratification, we aim at assessing how an explicit fast ice representation included in a model affects the simulation of the ice shelf melt rate evolution between the last decades and the end of the 21st century. In order to answer these questions, we designed ~~four~~ six simulations with a high-resolution, regional configuration of the NEMO3.6-LIM3 model, ~~two~~ four of them being forced with anomalies derived from a simulation with the global climate model EC-Earth3 driven by the SSP4-4.5 scenario (Shared Socioeconomic Pathways; Döscher et al., 2021).

This manuscript is organised as follows. The model, regional configuration and experimental design are described in Section 2. In Section 3, we analyse the changes in sea ice and ocean characteristics and ice shelf melt rate between the last decades and the end of the 21st century simulated by the model. The sensitivity of the ice shelf melt rate to the representation of fast ice is then addressed in Section 4. Conclusions are finally given in Section 5.

2 The model, forcing and experimental design

2.1 Ocean–sea ice model

We make use of NEMO 3.6 (Nucleus for European Modelling of the Ocean; Madec, 2008) that includes the ocean model OPA (océan parallélisé) coupled with the Louvain-la-Neuve sea ice model (LIM3; Vancoppenolle et al., 2009; Rousset et al., 2015). This combination is hereafter referred to as NEMO-LIM. OPA is a state-of-the-art, finite-difference ocean model based on primitive equations. Our setting includes a polynomial approximation of the seawater equation of state (TEOS-10, IOC, 2010) optimized for a Boussinesq fluid (Roquet et al., 2014). Vertical turbulent mixing is rendered through a Turbulent Kinetic Energy (TKE) scheme (Bougeault and Lacarrere, 1989; Gaspar et al., 1990; Madec et al., 1998). The enhanced vertical diffusion mixing coefficient utilised in this scheme is fixed to 20 m^2/s. LIM3 uses a five-category subgrid-scale distribution of sea ice thickness (Bitz et al., 2001). The drag coefficient is set to 7.1 $\times$ 10^{-3} at the sea ice–ocean interface and 2 $\times$ 10^{-3} at the sea ice–atmosphere one (Massonnet et al., 2014). Ice shelf cavities with explicit ocean—ice shelf interactions are represented by the ice shelf module implemented in NEMO by Mathiot et al. (2017), using the three-equation formulation from Jenkins (1991). Transfer coefficients for heat (γ_T) and salt (γ_S) between the ocean and ice shelves are velocity dependent (Dansereau et al., 2014): $\gamma_{T,S} = \Gamma_{T,S} \times u_*$. The friction velocity is given by $u_* = C_d \times \sqrt{u_{TML}^2}$ and constant values of Γ_T and Γ_S taken from Jourdain et al. (2017) are employed ($\Gamma_T = 2.21 \times 10^{-2}$ and $\Gamma_S = 6.19 \times 10^{-4}$ for temperature and salinity, respectively). C_d is the top drag coefficient, set to ~~14×10^{-3}~~ 3×10^{-3}, and u_{TML} is the ocean velocity in the top mixed layer, which is either the top 30 m of the water column or the top model layer (if thicker than 30 m) (Losch, 2008).

2.2 The Totten24 model configuration

Here, we use a regional configuration of NEMO-LIM, referred to as Totten24, which is described in detail in Van Achter et al. (2022). The horizontal grid is a 1/24°refinement (less than 2 km grid spacing) of the eORCA1 tripolar grid, centered on the continental shelf in front of the TIS, East Antarctica, and covering an area between 108-129° E and 63-68° S (Fig. 1). The NEMO and LIM time steps are 150 s and 900 s, respectively. The vertical discretisation has 75 levels, with level thickness increasing with depth and partial cells used for better representing bedrock and ice shelf bases (Adcroft et al., 1997). The ocean layer directly underneath the ice shelf base varies between 30 m near the cavity front and 80 m in the center of the cavity. The bathymetry and ice shelf draft datasets are derived from the NASA Making Earth System Data Records for Use in Research Environments (MEaSUREs) program, which contains a bathymetry map of Antarctica based on mass conservation, streamline diffusion and other methods (Morlighem et al., 2020).

The ocean lateral boundary conditions and initial conditions are taken from a 1979-2014 simulation with an eORCA025 (1/4°, 75 levels) peri-Antarctic NEMO-LIM configuration (Pelletier et al., 2022) (hereafter referred to as PARASO). Because of a negative salinity bias in the PARASO simulation, a salinity correction of 0.25 g/kg is uniformly added to the ocean lateral boundary conditions and initial conditions. At the lateral boundaries, a flow relaxation scheme (Engedahl, 1995) is applied to the three-dimensional ocean variables and two-dimensional sea ice variables. A Flather scheme (Flather, 1994) is used for barotropic velocities and sea surface elevation. Furthermore, the sea surface elevation and barotropic velocities from the FES2014 tide model (Carrère et al., 2012) are added to the boundary for the tide components K1, K2, M2, P1, O1, S2, 2N2, Mm, M4, Mf, Mtm, MU2, N2, NU2, Q1, S1, L2, T2, as in Maraldi et al. (2013); Jourdain et al. (2019); Huot et al. (2021). The surface fluxes of heat, freshwater and momentum are computed using the CORE bulk formulas (Large and Yeager, 2004), with atmosphere input coming from the fifth generation ECMWF atmospheric reanalysis (ERA5, Hersbach et al., 2020). No surface salinity restoring is applied.

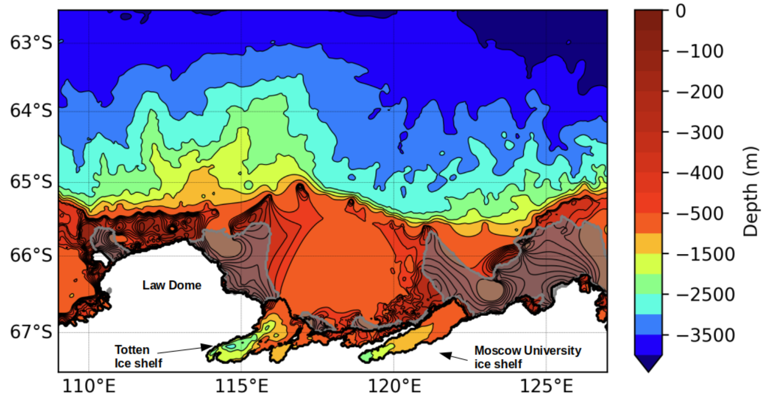

Figure 1. Model bathymetry and domain. The contour interval is 50 m up to 500 m depth and 500 m up to 4500 m depth. Ice shelf cavities are surrounded by a thick black line. The 0.75 fast ice observed frequency from Fraser et al. (2020) is shown by the shaded gray areas.

2.3 Experimental design

Our experimental design consists of one reference simulation and a set of ~~three~~ five sensitivity experiments. All simulations include the tide constituents and the ocean–ice shelf interactions (i.e., open ice shelf cavities and interactive basal melt computation). The reference simulation (REF) includes a representation of grounded icebergs and a sea ice tensile strength parameterisation. Both are needed to simulate adequately the fast ice formation (Van Achter et al., 2022). The grounded iceberg dataset used is extracted from the remote sensed mosaic 'RAMP AMM-1 SAR Image Mosaic of Antarctica, Version2' (Jezek et al., 2013) and covers the September-October months of 1997. The grounded icebergs are prescribed in the model by setting the bathymetry value to zero at every iceberg location ~~(see Van Achter et al. (2022))~~(Van Achter et al., 2022). The sea ice tensile strength parameterisation was developed by Lemieux et al. (2016). The REF simulation covers the 1995 to 2014 period, with a ~~1993-1994~~ 20 years spin-up. A similar simulation was conducted by Van Achter et al. (2022) and evaluated against observations (sea ice concentration, fast ice, sea ice production, sea ice thickness, polynya locations and temperature and salinity profiles). For the present study, the salinity bias identified in ~~this study~~ Van Achter et al. (2022) has been corrected (Fig. 2b), without altering the vertical profiles of temperature (Fig. 2a)~~, and the~~ . Moreover, due to a miscalculation in Van Achter et al. (2022) in the computation of the temporal basal melt rate, the top drag coefficient in the ice shelf cavities has been ~~increased~~ decreased from 8×10^{-3} to ~~14×10^{-3} to reduce the ice shelf melt rate bias~~3×10^{-3}. With these modifications, the simulated TIS melt rate (~~9.06~~ 11.13 m/yr) is in better agreement with Rignot et al. (2013)'s estimate (10.47 $\pm$ 0.7 m/yr). ~~This is also the case for the Moscow University ice shelf (MUIS), with a simulated melt rate of 5.95 m/yr, which is closer to the 4.7 $\pm$ 0.8 m/yr estimate of Rignot et al. (2013).~~ Except for those changes in ice shelf melt rate and salinity profiles, results from this new REF simulation are very similar to those of the previous one in terms of sea ice distribution and ocean circulation.

The sensitivity experiments include the nFST, WARM and nFST_WARM simulations (Table 1). nFST is identical to REF but without fast ice representation i.e., no tensile strength parameterisation and no grounded icebergs representation. WARM and nFST_WARM have the same setup as REF and nFST, respectively, but cover the 2081-2100 period. In these simulations, the model is forced by climate anomalies derived from a climate change projection carried out with the global climate model EC-Earth3 under the SSP4-4.5 scenario (Döscher et al., 2021), within the 6th phase of the Coupled Model Intercomparison Project (Eyring et al., 2016). Note that, in WARM, the grounded icebergs location are the same as in REF~~.~~, and that, as for REF and nFST, WARM and nFST_WARM have a 20 years spin-up. Two more sensitivity experiments have been conducted to disentangle the effect of both the atmospheric and oceanic forcing on the ASC acceleration. WARM_noAtm is similar to WARM, except that this simulation has no EC-Earth3 anomaly applied over the atmosphere. WARM_noOce is equivalent to WARM but without the EC-Earth3 anomaly applied over the ocean velocity.

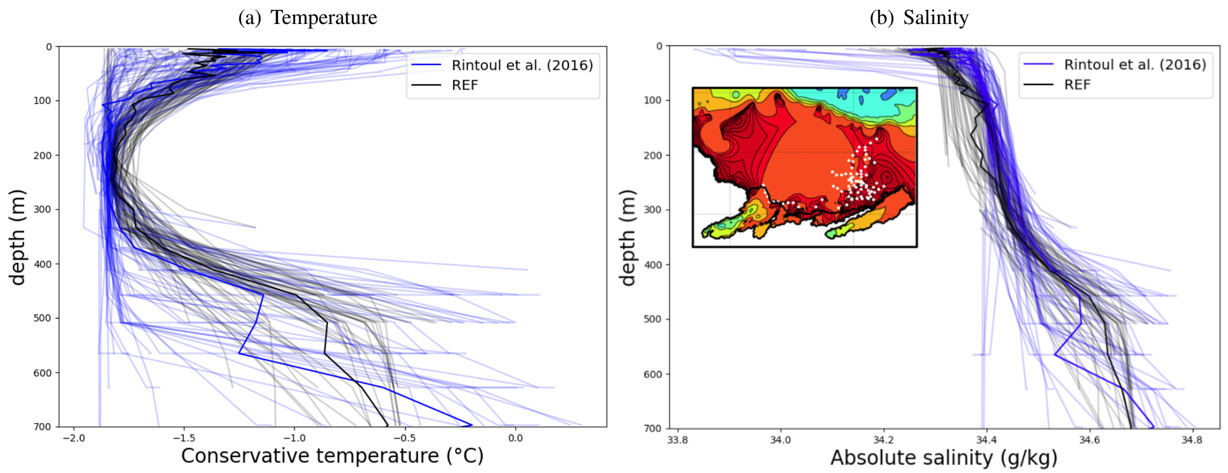

Figure 2. Vertical profiles of temperature (a) and salinity (b) after the bias correction on the continental shelf in front of the Totten ice shelf. Blue: CTD from Rintoul et al. (2016) (a1402). ~~Red~~Black: as simulated in REF. Simulated profiles are taken at the same time and location as the CTD measurements. The observations have been collected in two locations, close to the TIS front and near the Dalton coastal polynya. The locations are denoted by white dots in the panel displayed in subfigure b.

Annual cycles of the EC-Earth3 climate anomalies are computed as the differences between 2081-2100 and 1995-2014, and are added to all the fields of the atmospheric and oceanic forcings used for the 1995-2014 period in REF and nFST (for the atmosphere: wind velocity, temperature, specific humidity, surface downward radiation and precipitation; for the ocean: current velocity, temperature, salinity, sea surface height, sea ice concentration, sea ice thickness and snow thickness). Figure 3 shows the annual mean ocean temperature, salinity and zonal ocean velocity anomalies at the eastern boundary condition, and the mean near-surface (2 m) air temperature and atmospheric zonal wind (10 m) velocity anomalies. We show the ocean anomalies at the eastern lateral boundary condition as they are very similar to those at the western lateral boundary condition, and also because the ocean eastern boundary condition is one of the drivers of the ocean dynamic over the continental shelf in regional modelling (Nakayama et al., 2021). The ocean temperature anomaly is positive everywhere, with values from 0 to 0.5° C over the continental shelf and in the deep ocean, and from 1 to 1.5° C in the upper ocean outside of the shelf. The seawater salinity anomaly is mostly negative (down to -0.4 g/kg), with the lower values above the continental shelf. Oceanic zonal velocity anomalies at the eastern boundary are westward over the shelf and eastward off the shelf. The EC-Earth3 anomaly applied at the zonal wind component is mostly eastward over the ocean, increasingly towards the north. Westward ~~winds anomaly~~ wind anomalies also occur, but only over a small part of the shelf and over the continent. The surface air temperature anomaly is positive everywhere (Fig 3e), with values larger than 1° C and up to 1.8° C near the coast.

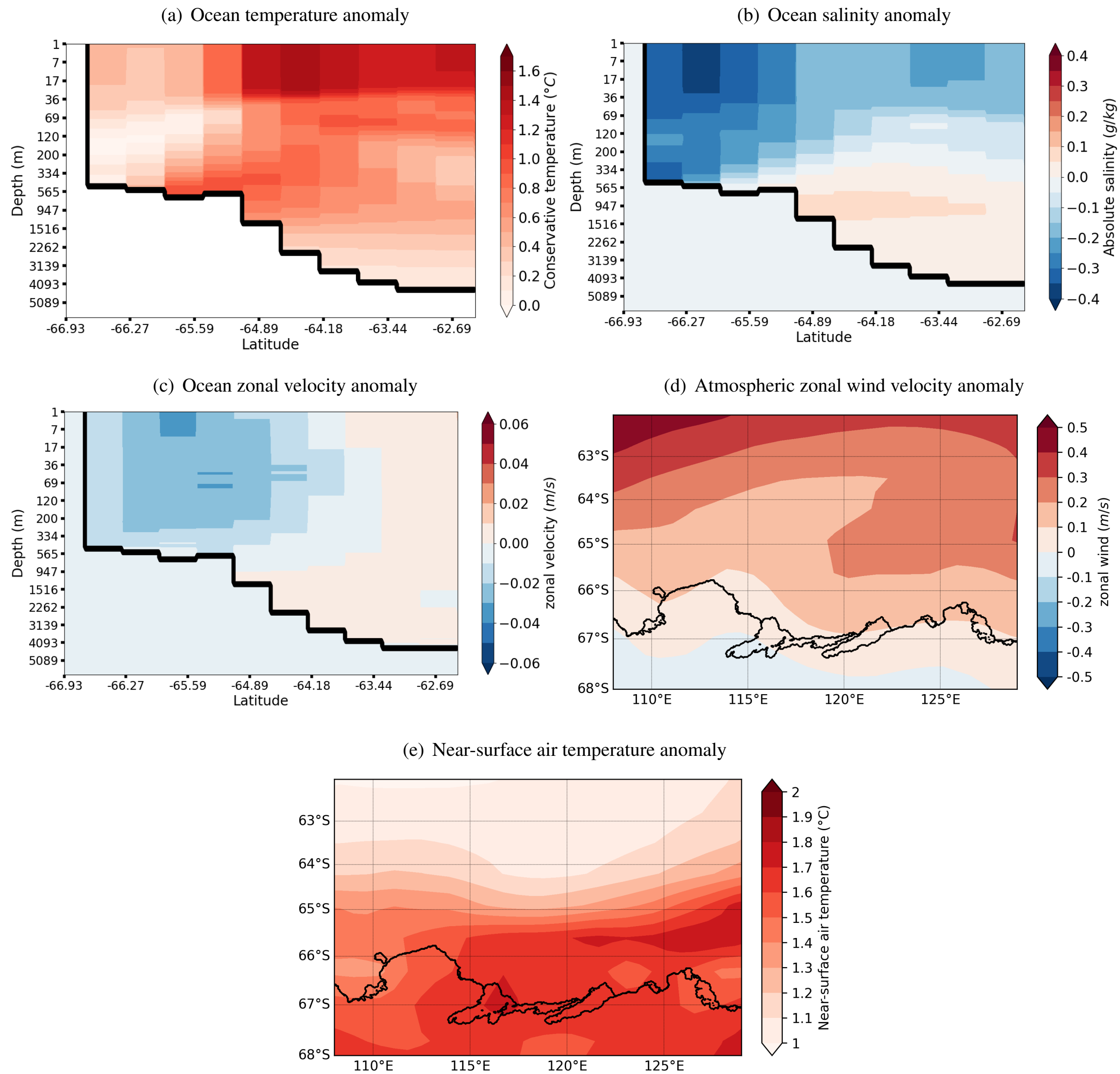

Figure 3. Annual mean EC-Earth3 anomalies applied at the eastern boundary of the model domain for the conservative temperature (a), absolute salinity (b) and the zonal component of the ocean velocity (c). Annual mean EC–Earth3 anomaly of the wind velocity (10 m) zonal component (d) and the near-surface (2 m) air temperature (e). The anomaly are computed between the 2081-2100 and the 1995-2014 periods.

	Landfast ice	Forcing and lateral boundary conditions
REF	yes	Last decades (ERA5, PARASO, 1995-2014)
WARM	~~no~~ yes	REF + anomalies derived from EC–Earth3 climate change projection
nFST	~~yes~~ no	Last decades (ERA5, PARASO, 1995-2014)
nFST_WARM	no	REF + anomalies derived from EC–Earth3 climate change projection
WARM_noAtm	yes	WARM - atmospheric anomalies derived from EC–Earth3 climate change projection
WARM_noOce	yes	WARM - ocean velocity anomaly derived from EC–Earth3 climate change projection

Table 1. Names and descriptions of the simulations used in this study.

3 Results

In this section, we examine the main differences between the results from the REF and WARM simulations. Figures 4a and 4b display the geographical distribution of the fast ice frequency, defined as the percentage of days in a year with a 2-week mean sea ice velocity lower than 0.005 m/s. There is a large retreat of fast ice in WARM compared to REF in front of both the TIS and MUIS. In front of the TIS, the multiyear fast ice cover (frequency above 0.9) in REF is replaced by first year fast ice in WARM. On the other hand, the first year fast ice (frequency between 0.4-0.8) in REF is not at all present in WARM. The same frequency decrease occurs in front of the MUIS, most of the multiyear fast ice in REF becomes first year fast ice in WARM, with a 50% frequency reduction, and the first year fast ice in REF has vanished in WARM. The loss of the multiyear fast ice in WARM is mainly due to the atmospheric forcings, as hinted by the fast ice simulated in WARM_noAtm presented in Figure A1, which is closer in both frequency and area to the fast ice simulated in REF than in WARM. As shown by Figure 4c to 4f, the changes in sea ice concentration over the continental shelf between REF and WARM mostly occur during summer months. In winter, changes are limited to the region off the continental shelf, with a general southward retreat of the ice edge in WARM.

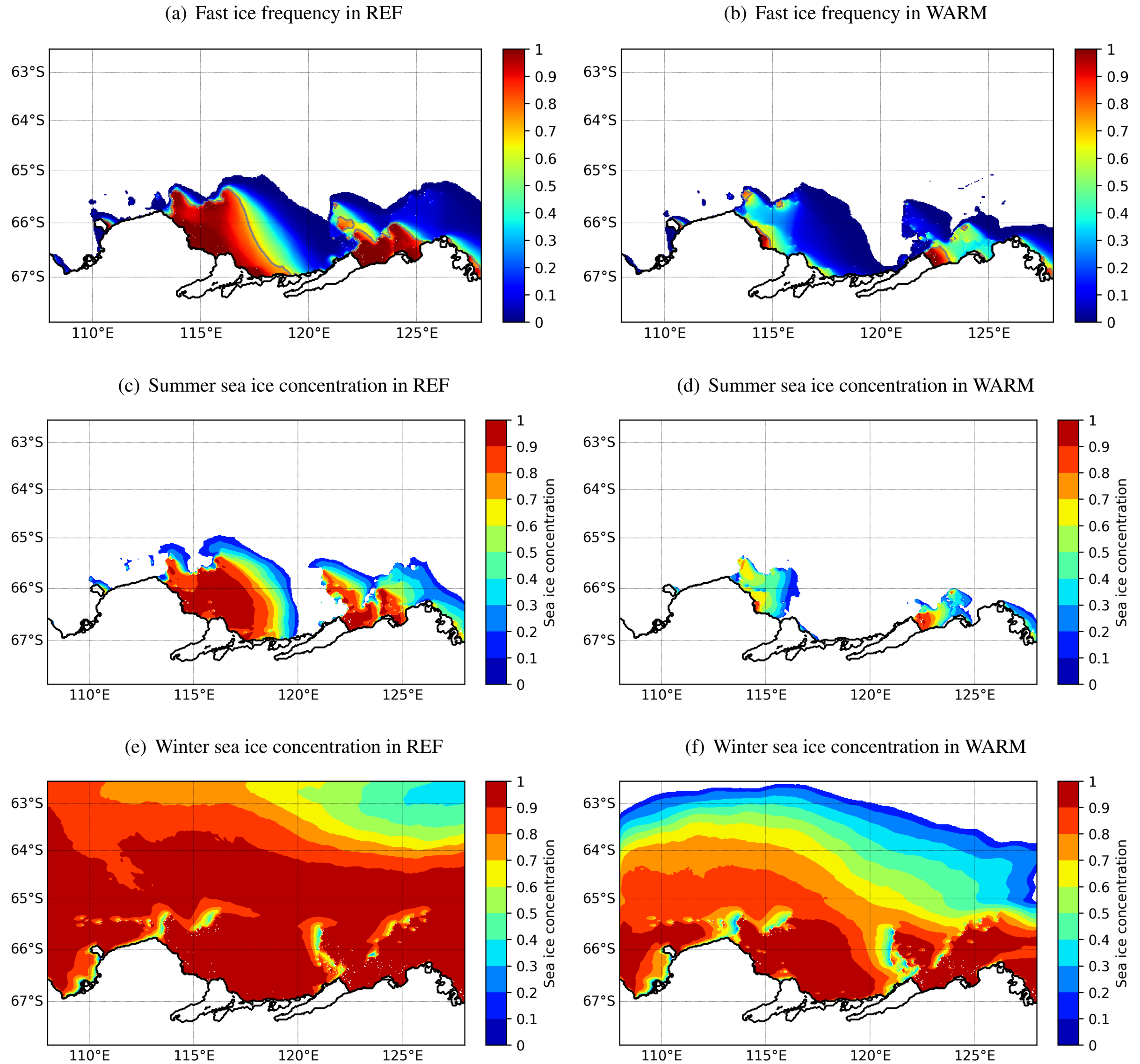

Figure 4. Fast sea ice frequency and sea ice concentration in summer (JFM) and winter (JASO) for the REF (left) and WARM (right) simulations, both averaged over the 20 years of ~~simulations~~simulation. The 0.75 fast ice frequency is shown by the gray line.

The differences in mean sea ice production between both simulations (see Fig. 5) exhibits important changes in sea ice production related to the fast ice changes presented above. The partial disintegration of multiyear fast ice in WARM induces more interactions between the cold atmospheric air and the ocean surface, which increases the sea ice production near the coast. This increase of sea ice production along the coast in WARM is counterbalanced by the decrease of sea ice production off shore, on the western side of the large fast ice packs that are present in REF but not in WARM.

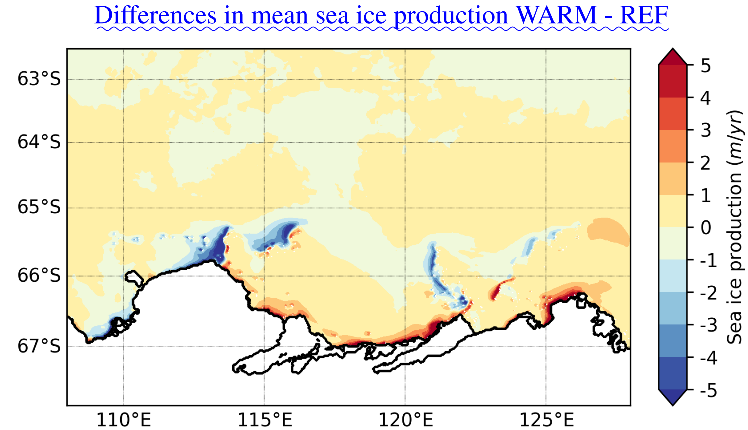

Figure 5. Differences in mean sea ice production between WARM and REF, averaged over the 20 years of simulations. Positive values mean that WARM has more sea ice production than REF.

Figures 6a and 6b reveal that the ocean circulation experiences major changes between REF and WARM. The ASC, which is barely present in REF, is strongly enhanced in WARM, especially in front of Law Dome and in front of the MUIS (the mean ocean velocity at the ASF is less than 0.1 m/s in REF and is close to 0.15 m/s in WARM). Furthermore, the Totten oceanic gyre in front of the TIS (clockwise oceanic circulation over the shelf) is intensified in WARM, especially its western and ~~northern~~ southern components. This acceleration mainly results from the retreat of fast ice, which acts as a dynamically isolating cover that inhibits the transmission of wind stress to the ocean ~~.~~ (as suggested in Fig. A2). The integrated ocean transport at the southern edge of the gyre, near the front of the TIS cavity is increased by 226% in WARM compared to REF (from 0.55 to 1.8 Sv). This accelerated gyre speeds up the ocean masses entering the TIS cavity, which partly contributes to the increased basal melting. Figure 6c shows the annual mean, depth-integrated zonal oceanic volume transport for ~~both REFand WARM~~the REF, WARM, WARM_noAtm and WARM_noOce simulations. For each simulation, this mean transport is westwards everywhere (positive value) from the coast until 63°S, with a maximum value near 65°S where the ASC is located (at the shelf break). The ~~eastern~~ eastward transport north of 63°S is associated with the Antarctic Circumpolar Current (ACC). REF and WARM exhibit the same transport pattern, but with a ~~90% increase~~ 116% increase of the ASC in WARM compared to REF.

~~The~~ As suggested by the similar pattern of westward ocean transport between WARM and WARM_noAtm (see Fig. 6c), the ASC intensification in WARM is not wind-driven. Indeed, as the pressure gradient across the ASF is enhanced by easterly winds that drive the sea surface height gradient via Ekman drift (Mathiot et al., 2011), an ASC intensification would required stronger easterly winds. Nevertheless, the EC-Earth3 wind velocity anomalies applied to the model in WARM are mostly positive (Fig. 3d), which weakens the easterly winds. ~~This suggests a~~ The ASC intensity difference between WARM and WARM_noOce in Figure 6c indicates that the ocean velocity anomaly derived from EC-Earth3 and applied to the oceanic forcing in WARM are responsible for 83% of the ASC increased intensity. The remaining 17% of ASC increased intensity could have a density-driven ~~origin for the ASC acceleration~~origin, as the lateral density gradient across the ASF contributes to establishing the geostrophically balanced, vertically sheared along-slope flows of the ASC (Lockwood et al., 2021). This is coherent with the large density lowering over the continental shelf in WARM compared to REF, which leads to a stronger density gradient across the ASF (Fig. 6d). Since the seawater density is mostly a function of salinity in the Southern Ocean (Pellichero et al., 2018), the ASC modification should then be linked to the changes in sea ice production and melt occurring in WARM. ~~This~~ These changes, in addition to the EC-Earth3 salinity anomalies prescribed at the eastern boundary of the domain (Fig. 3b), reduce the ocean salinity over the shelf.

As hinted by Nakayama et al. (2021), the ASC modulates the heat intrusion towards the continental shelf and the ice shelf cavities. The basal melt rate for both cavities for WARM and WARM_noOce (see Fig. A3) shows higher melt rate with low ASC intensity (WARM_noOce) and lower melt rate with high ASC intensity (WARM). This implies that, whereas the ocean and surface air temperature increase induces more basal melt rate, the ASC increased intensity decreases the heat intrusion towards the ice shelf cavities and limits the basal melt increase.

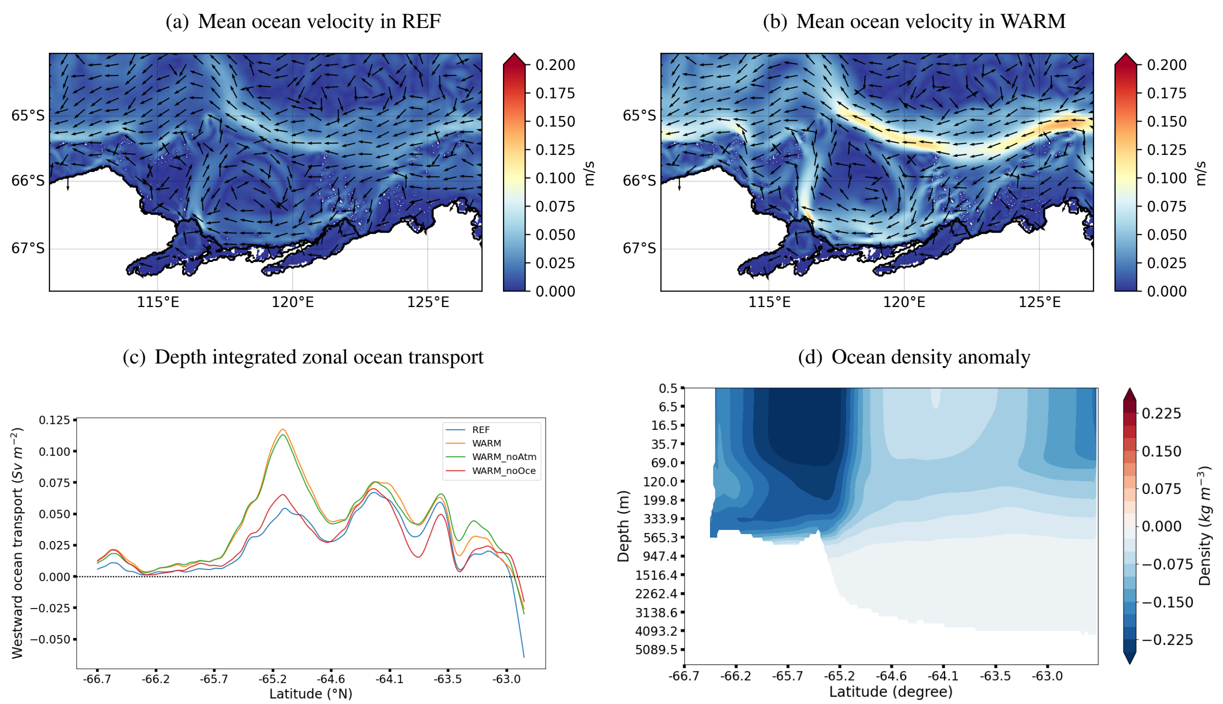

Figure 6. Annual mean, depth-averaged ocean velocity for the REF (a) and WARM (b) simulations, both averaged over the 20 years of simulation. (c) Annual mean, depth-integrated zonal ocean volume transport. (d) Meridional section of the ocean density change between WARM and REF~~(averaged over 125.3-126.6 E)~~.

Figure 7 depicts the annual mean ocean temperature differences between WARM and REF (WARM - REF) over the continental shelf at 200, 300, 400 and 500 m depth. Despite an intensified ASC, which tends to isolate the continental shelf from the open ocean by reducing the across-shelf exchanges, the ocean temperature over the continental shelf in WARM features an overall increase. Figure 7a shows warmer water mostly everywhere at 200 m, with a slight warming (from 0.1 to 0.4° C) over the shelf and a larger warming (from 0.4 to 1° C) in the open ocean. Cooler waters are found on the eastern flank of the

MUIS cavity (from 0 to $-0.2°$ C). The same pattern of temperature difference is noticed at 300 and 400 m (Fig. 7b and 7c), with a slight cooling next to MUIS and a strong warming in front of TIS, inside the Totten oceanic gyre, where the temperature increase reaches more than $+1°$ C. Deeper, at 500 m, the temperature difference in front of the MUIS becomes positive (up to $+0.2°$ C), and the cooling in front of the MUIS is now restricted to the region east of 126°E (Fig. 7d). The difference of ocean warming between the front of the TIS and the front of MUIS is mostly due to the differences in bathymetry in the two areas. Indeed, both ice shelves present the same warmer ocean masses at the shelf break but ~~only~~ the deeper bathymetry in front of the TIS (up to 600 m) allows ~~the~~ more warming to reach the TIS cavity.

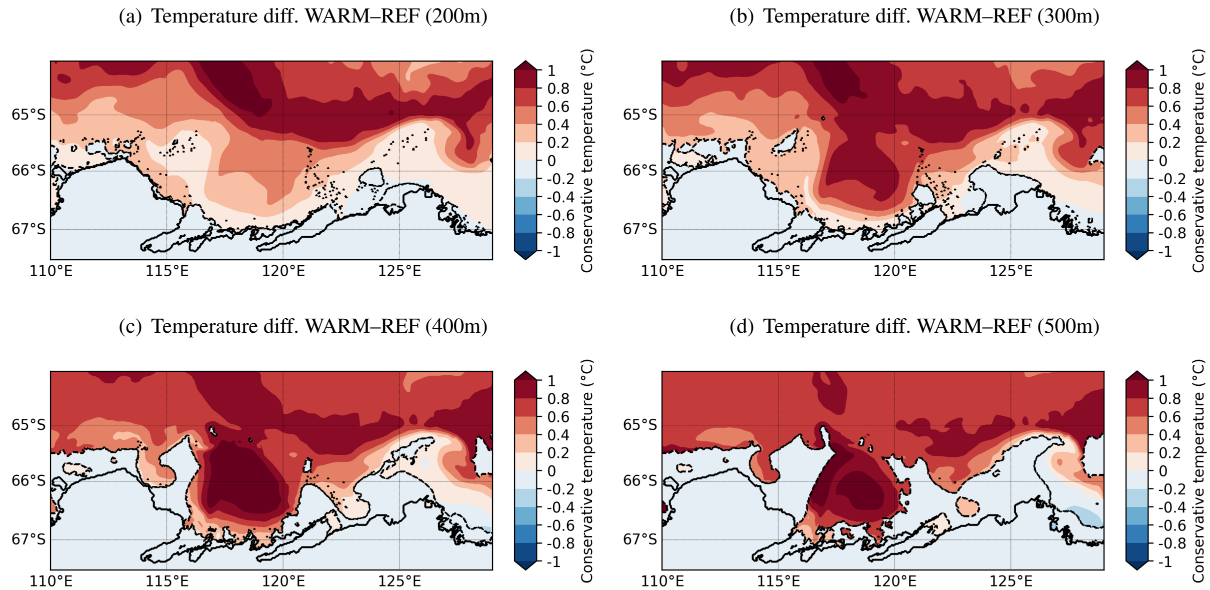

Figure 7. Annual mean ocean temperature differences between the WARM and REF simulations over the continental shelf at 200, 300, 400 and 500 m depths, all averaged over the 20 years of simulation. The dashed line depicts the contours of the bottom topography.

Finally, ~~Figure 8displays~~ Figures 8a and 8b display the area-averaged ice shelf basal melt rate for both the TIS and MUIS from REF and WARM. The TIS experiences a larger (+~~41%~~91%) and more variable (+~~55%~~130% in standard deviation) basal melt rate in WARM ~~,~~ compared to REF. By contrast, the MUIS basal melt rate ~~is almost the same in both simulations (less than 1%~~ exhibits a lower basal melt rate increase (+36% increase in WARM) ~~, which~~ with a lower basal melt rate variability increase (+33% in standard deviation). The lower basal melt increase in MUIS can be attributed to the lower ocean warming in front of the MUIS cavity, with less than +0.2° C in front of MUIS compared to more than $+1°$ C in front of the TIS (see Figure 7). The increased temporal variability of both TIS and MUIS basal melt rates in WARM in not related to the loss of fast ice (see Tab. 2), but could be explained by the larger Mixed Layer Depth (MLD) variability in front of the cavities in WARM (see Fig. A4). This higher MLD variability is related to the greater amplitude of the surface air temperature seasonal cycle. The mixed layer in front of the cavity, by its impact on the ocean stratification, modulates the amount of warm water entering the cavities (Van Achter et al., 2022). The drop of basal melt rate in the sixth and seventh years is inherent to the ocean boundary conditions. Figure 8c shows the differences in spatial distribution of the mean basal melt rate inside the TIS and MUIS cavities between both simulations. The melt rates increase spans from few meters a year to more than 45 meter of ice per year. The highest basal melt rate increase between REF and WARM are located on the western side of each cavities, near the grounding line, where the ocean circulation within the cavities is the fastest (up to +45m/yr in Totten and up to +20 m/yr in MUIS).

(a) Area-averaged TIS basal melt rate

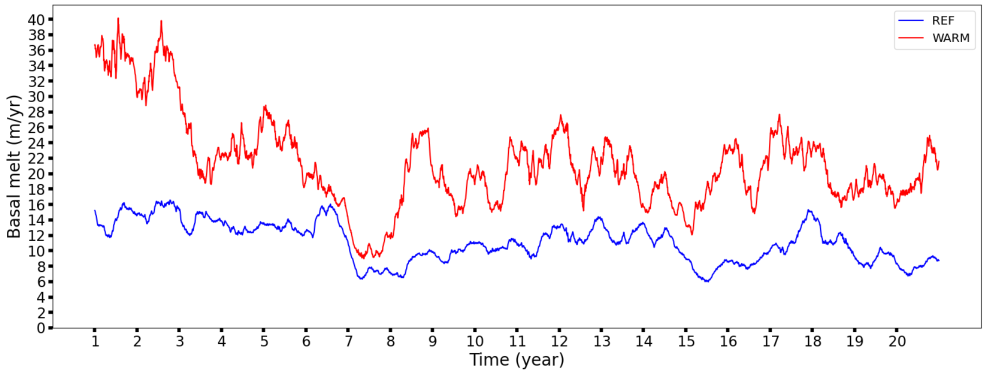

(b) Area-averaged MUIS basal melt rate

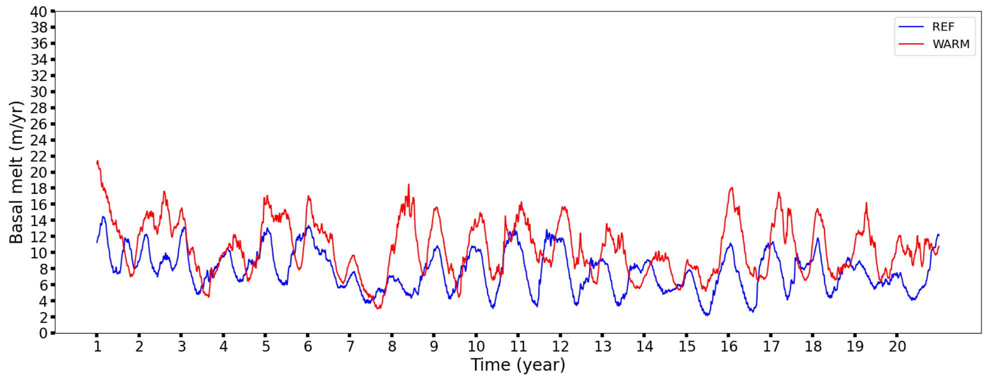

(c) Differences in basal melt rate WARM-REF

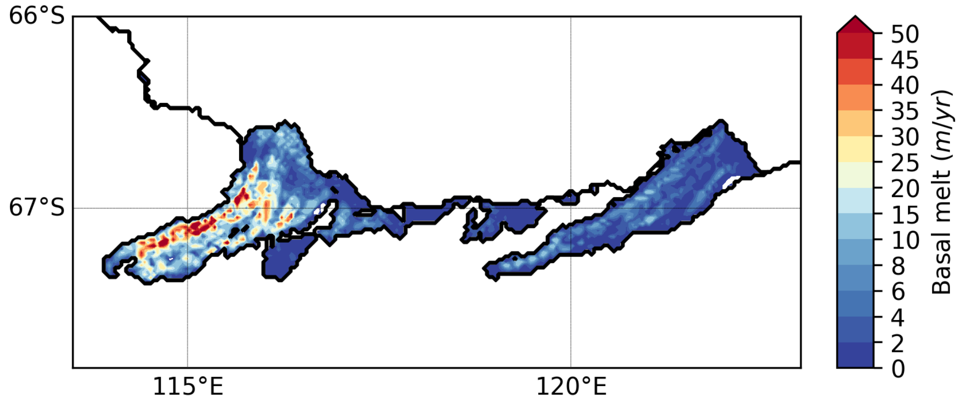

Figure 8. Time series of the area-averaged TIS (a) and MUIS (b) basal melt rates from REF (blue) and WARM (red). Differences in spatial distribution of the basal melt rate between the REF and WARM simulations. The time periods are 1995-2014 for REF and 2081-2100 for WARM. The mean TIS basal melt rate is ~~9.06~~ 11.13 ± ~~4.64~~ 2.54 m/yr in REF and ~~12.8~~ 21.29 ± ~~11.19~~ 5.88 m/yr in WARM, while the MUIS basal melt rate is ~~5.9~~ 7.73 ± ~~5.42~~ 2.51 m/yr in REF and ~~5.95~~ 10.51 ± ~~3.37~~ 3.35 m/yr in WARM.

4 Ice shelves melt rate sensitivity to fast ice in a warming climate

In this section, we analyse how the presence of fast ice, implemented through the combination of both a sea ice tensile strength parameterisation and a representation of grounded icebergs, impacts the changes in ice shelf basal melt rate between the last decades and the end of the 21st century. The area-averaged TIS and MUIS basal melt rates for both nFST and nFST_WARM are shown in Figure 9. The TIS has a basal melt rate of ~~8.09~~ 8.74 ± ~~3.08~~ 2.76 m/yr and ~~12.78~~ 20.68 ± ~~13.34~~ 5.87 m/yr in nFST and nFST_WARM, respectively, whereas the MUIS has a mean basal melt rate of ~~4.67~~ 6.28 ± ~~2.6~~ 2.25 m/yr and ~~6.44~~ 11.01 ± ~~9.18~~ 4.67 m/yr in nFST and nFST_WARM, respectively.

(a) Area-averaged TIS basal melt rate

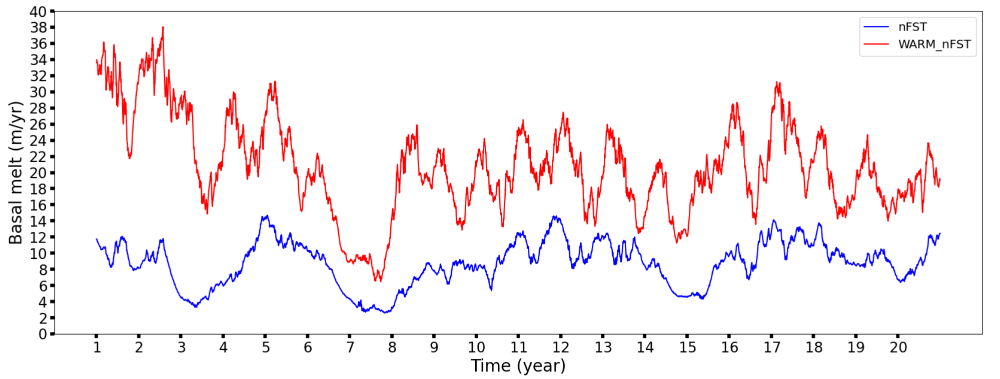

(b) Area-averaged MUIS basal melt rate

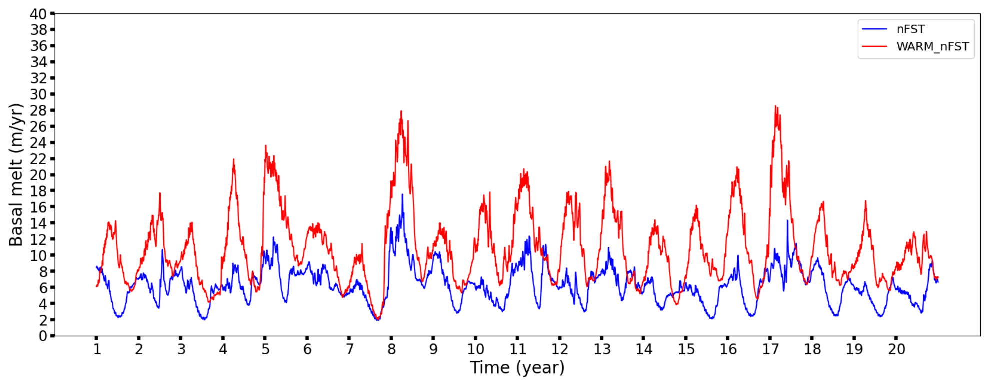

Figure 9. Time series of the area-averaged TIS (a) and MUIS (b) basal melt rates from nFST (blue) and nFST_WARM (red). The timescale are 1995-2014 and 2018-2100 for the last decades simulations (blue) and the future climate conditions (red), respectively. The time period are 1995-2014 for nFST and 2081-2100 for nFST_WARM. TIS melt rate are ~~8.09~~ 8.74 ± ~~3.08~~ 2.76 m/yr in nFST and ~~12.78~~ 20.68 ± ~~13.34~~ 5.87 m/yr in nFST_WARM. MUIS melt rate are ~~4.67~~ 6.28 ± ~~2.6~~ 2.25 m/yr in nFST and ~~6.44~~ 11.01 ± ~~9.18~~ 4.67 m/yr in nFST_WARM.

The mean melt rates at the base of the TIS and MUIS for all simulations are given in Table 2. Without fast ice representation, the increase in basal melt rate for both ice shelves between the two time periods is much larger. This is explained by both the strong impact of fast ice on the ice shelf basal melt rate ~~. Indeed, through the displacement of~~ for the last decades simulation (more than 1.45 m/yr between REF and nFST) and by its small impact on the ice shelf basal melt rate by the end of the 21st century (less than 0.6 m/yr between WARM and WARM_nFST). The strong fast ice impact on the basal melt rate in the last decades simulations is related to the displacement of the sea ice production zones (see Fig. A5), by the fast ice, from coastal to offshore areas~~, the presence of fast ice~~. This change of sea ice production induces less sea ice production and more sea ice melt near the coast, which increases the ocean stratification in front of the cavities, favors warm water intrusions and increases the basal melt rate in REF compared to nFST (Van Achter et al., 2022). However, as the fast ice ~~disappears~~ shrinks under warmer oceanic and atmospheric conditions of the 21st century (Fig. 4a and 4b), this fast ice impact on the basal melt rate is strongly reduced. So, with lower ice shelf melt rates in nFST than in REF but with ~~similar melt rates in~~ no significant melt rate changes between WARM and nFST_WARM, the simulations without a fast ice representation are showing a stronger ice shelf melt rate growth between the two periods. In other words, the effect of the reduced extent of fast ice on the ice shelf basal melt rate offsets part of the melt rate increase due to warmer atmospheric and oceanic conditions.

Ice shelves	fast ice	last decades (1995-2014)	end of the 21st century (2081-2100)
Totten	yes	~~9.06~~ 11.13 ± ~~4.64~~ 2.54 m/yr	~~12.8~~ 21.29 ± ~~11.19~~ 5.88 m/yr (+~~41%~~91%)
	no	~~8.09~~ 8.74 ± ~~3.08~~ 2.76 m/yr	~~12.78~~ 20.68 ± ~~13.34~~ 5.87 m/yr (+~~58%~~136%)
Moscow University	yes	~~5.9~~ 7.73 ± ~~5.42~~ 2.51 m/yr	~~5.95~~ 10.51 ± ~~3.37~~ 3.35 m/yr (+~~1%~~36%)
	no	~~4.67~~ 6.28 ± ~~2.6~~ 2.25 m/yr	~~6.44~~ 11.01 ± ~~9.18~~ 4.67 m/yr (+~~38%~~75%)

Table 2. Mean ice shelf basal melt rates for both the last decades and the end of the 21st century and for all simulations.

~~The TIS and MUIS basal melt rates present a different sensitivity to fast ice. This is explained by both the unchanged MUIS basal melt rate in WARM compared to REF, and the higher MUIS basal melt rate in nFST_WARM compared to WARM. Combined, these two effects contribute to a much larger basal melt rate increase between the simulations with and without fast ice for the MUIS than for the TIS (difference of 37% in melt rate increase for MUIS and 17% for TIS). The unchanged MUIS basal melt rate in WARM compared to REF is attributed to the limited effect of the ocean warming over the MUIS cavity, whereas the warmer ocean masses reaches the TIS cavity (Fig. 7d). This is explained by the differences in bathymetry in front of each ice shelf cavity. As described in Van Achter et al. (2022), in REF, the mCDW only reaches the TIS (not the MUIS), which results in an enhanced TIS basal melt rate and a lower MUIS melt rate. In the same way, in WARM, the warmer water masses reach the TIS, but are limited outside of the MUIS cavity, which limits the MUIS basal melt rate changes between REF and WARM.~~ Finally, the higher MUIS basal melt rate in nFST_WARM compared to WARM is attributed to the changes affecting the sea ice in WARM and nFST_WARM. In nFST_WARM, the absence of fast ice allows strong sea ice formation along the coast, with a deep ~~mixed layer depth (mld)~~ MLD in front of the MUIS cavity (Fig. 10c). In contrast, in WARM, the presence of fast ice allows for sea ice formation ~~along the coast but also~~ at the off-shore polynya created on the west side of fast ice patches in front of the MUIS cavity, but it also allows strong sea ice production along the coast since the fast ice along the coast is strongly reduced in area and frequency. This combination of sea formation both off-shore and along the coast contributes to a broader area of deep ~~mld~~ MLD in front of the MUIS cavity in WARM (Fig. 10d), which decreases the amount of warm water able to cross the continental shelf and to reach the MUIS cavity in WARM compared to nFST_WARM (Fig. 10a and 10b). As a consequence, the MUIS basal melt rate in WARM is lower than in nFST_WARM.

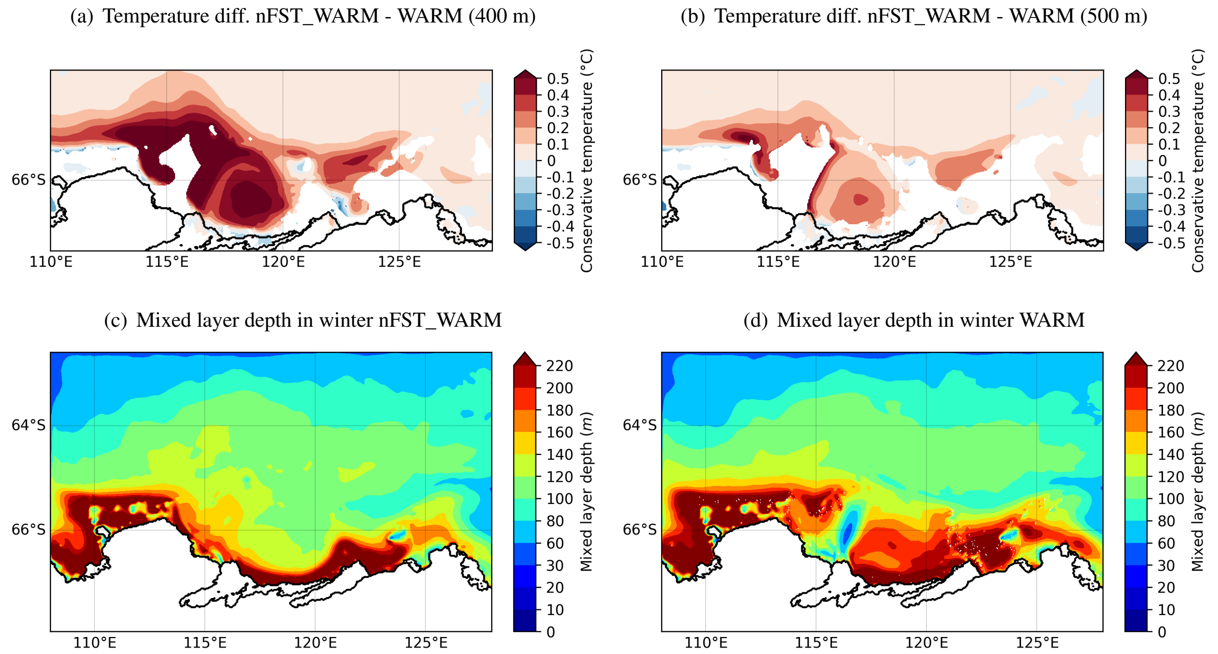

Figure 10. Annual mean ocean temperature differences between the nFST_WARM and WARM simulations over the continental shelf at 400 (a) and 500 m depths (b). Annual mean ~~mld~~ MLD for nFST_WARM (c) and WARM (d) for the winter months (JASO). Both the temperature anomalies and the ~~mld~~ MLD are averaged over the 20 years simulation.

5 Discussion and conclusions

The first goal of this study was to investigate the ocean–ice shelf interactions under warmer climate conditions in the Totten Glacier region. To do so, we applied climate anomalies, obtained from a SSP4-4.5 climate change projection conducted with EC-Earth3, at the oceanic boundary conditions and atmospheric forcing of a NEMO-LIM high-resolution, regional configuration, which includes an explicit treatment of ocean–ice shelf interactions and a fast ice representation. Our experiments revealed major changes in ice shelf basal melt rate, sea ice production and ocean circulation between last decades (1995-2014) and the end of the 21st century (2081-2100). The ~~TIS undergoes~~ sea ice extent is reduced in both summer and winter, with a general southward retreat of the ice edge. The fast ice forms less frequently and its coverage is strongly reduced. Both TIS and MUIS underwent a drastic basal melt increase ~~(41%), while the MUIS basal melt rate remains almost unchanged (less than 1% increase)~~with a 91% and 36% increase, respectively. Such change in the ~~TIS~~ ice shelf basal melt rate can be attributed to warmer mCDW~~(~~, with more than $+1°C$ ~~) reaching its cavity . On the other hand, these~~ of ocean warming in front of the TIS cavity and up to $+0.2°C$ in front of the MUIS cavity. The warmer ocean conditions ~~do not affect~~ have a lesser effect on the MUIS basal melt rate, mainly because of the shallower bathymetry in front of its cavity~~(less than $+0.2°C$). The warmer atmospheric and oceanic conditions strongly impact the sea ice in the projection run. The fast iceforms less frequently and its coverage is strongly reduced. The sea ice extent is also reduced in both summer and winter~~, but also because of the accelerated gyre in front of the TIS cavity, whose acceleration is due to the disintegration of fast ice. This accelerated gyre speeds up the ocean masses entering the TIS cavity and contributes to the basal melt rate increase. In the ocean, the ASC is largely intensified, with an oceanic zonal volume transport ~~almost twice larger in WARM than in REF. The~~ that is increased by 116% in WARM compared to REF. This increase velocity of the ASC ~~seems to be due to the change~~ is attributed to both the EC-Earth3 ocean velocity anomaly applied to the ocean forcings (83%) and to the changes in density gradient (mostly salinity) across the shelf (17%), triggered by both the sea ice production modification and the changes in ocean lateral boundary conditions. The accelerated ASC reduces the cross-slope water exchanges and has a basal melt rate reducing effect in both ice shelf cavities.

The second goal of this study was to determine how fast ice influences the increase in ice shelf basal melt rate between the last decades and the end of the 21st century. The representation of fast ice, through the combination of both a sea ice tensile strength parameterisation and the representation of grounded icebergs, has been shown to offset the basal melt rate increase simulated between the last decades and the end of the 21st century. Indeed, for ~~both the TISand MUIS~~the TIS, the average last decades melt rates are higher with the fast ice representation but ~~are similar~~ have no significant differences by the end of the 21st century, whether or not there is the fast ice representation. For MUIS, it is a similar case, except that the end of the 21st century basal melt rate is slightly lower with the fast ice representation due to spatial changes in the MLD. The fast ice impact on the melt rate drops as the fast ice extent is reduced due to the warmer oceanic and atmospheric conditions by the end of the 21st century. So, with higher melt rate values for the last decades, but with similar melt rate values by the end of the 21st century, the simulations with fast ice have a lower melt rate growth between the two periods than the simulations without a fast ice representation. This enlightened the importance of fast ice, not for studying melt rate by the end of the 21st century alone, but for studying the evolution of basal melt rate across the 21st century.

Few other studies investigate the ice shelf melt rate increase between present days and the end of the 21st century in the Totten Glacier area. Moreover, the amount of melt rate increase is strongly linked to the model, initial conditions and climate change scenario used to force the model. ~~Pelle et al. (2021) simulate a TIS basal melt rate increase of 56% following a high emission scenario, which compares well with our 58% TIS basal melt rate increase (without fast ice). Nevertheless, their simulations present an ASC weakening linked to a freshening at the eastern ocean model boundary, which is the opposite of what we observe in WARM. As~~ Furthermore, as recent studies are suggesting both strengthening and weakening of the ASC in the future (Moorman et al., 2020; Pelle et al., 2021), we should aim for better understanding of the ASC changes in East Antarctica.

One of the main limitations of our study lies in the lack of knowledge about the grounded iceberg distribution by the end of the 21st century. In the absence of a day-to-day high-resolution iceberg map, we ~~were forced to use~~ used a 2-month icebergs dataset (September–October months of 1997) to prescribe the grounded iceberg location for both the REF (1995-2014) and WARM (2081-2100) simulations. However, a change in the iceberg distribution between REF and WARM might influence the results presented here. Indeed, a modification of the iceberg density in front of the TIS and MUIS cavities could either increase or decrease the fast ice distribution over the continental shelf, and consequently influence how the fast ice change damps the ice shelf basal melt rate under warming conditions. Another limitation in our experimental design, is the use of only one climate change projection. Still about the experimental design, the REF and WARM simulations have the same interannual variability (because WARM is REF with EC–Earth3 anomalies). A WARM simulation with its own interannual variability might change how the TIS and MUIS basal melt rates are enhanced in WARM. ~~Finally~~Moreover, since these results are strongly linked to local processes, it would be interesting to look at the same mechanisms but in other regions of East Antarctica. Finally, ASC analysis should be made on a wider scale and on other regions. Because, even if the ASC intensification in WARM is not wind-driven, the winds outside of the local domain should be part of the ASC driven force.

Overall, the ~~density-driven ASC acceleration highlights the~~ ASC acceleration and its effect on the basal melt rate highlight the benefits of high-resolution and accurate continental shelf bathymetric datasets in order to represent lateral density gradients associated with the ASF, and thus to simulate realistically the ASC. This is a major challenge for global climate models, whose relatively coarse resolution prevents such phenomena from being accurately represented (Lockwood et al., 2021). Furthermore, our results underline the worth of a prognostic fast ice representation to simulate ~~future~~ ice shelf melt rate evolution in Antarctica. In contrast to the prescribed fast ice, the prognostic approach enables the fast ice extent to evolve in time (Nihashi and Ohshima, 2015; Van Achter et al., 2022). The prognostic representation of fast ice, with time-evolving grounded iceberg locations should be one of the key focus in high-resolution ocean-sea ice modelling in East Antarctica for the years to come.

Appendix A

Figure A1 presents the fast ice frequency in WARM_noAtm. As the fast ice frequency and area in WARM_noAtm are closer to the ones of REF that of WARM, it suggests that the changes in fast ice between REF and WARM are mainly due to the changes in atmospheric forcings between REF and WARM.

Fast ice frequency in WARM_noAtm

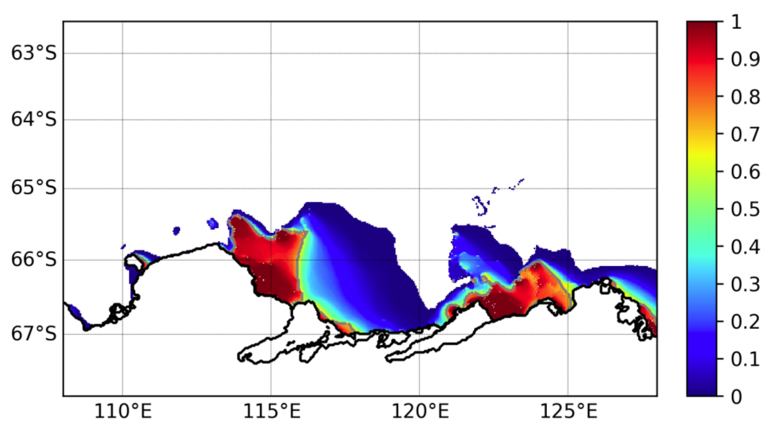

Figure A1. Fast ice frequency for the WARM_noAtm simulation, averaged over the 20 years of simulation.

Figure A2, which shows the mean ocean barotropic velocity for the REF and nFST simulations, suggests that the acceleration of the Totten oceanic gyre is related to the absence of fast ice in front of the TIS cavity.

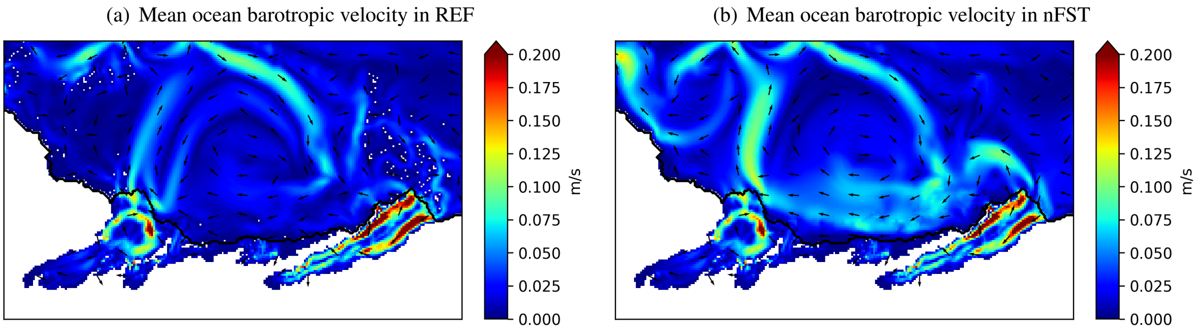

Figure A2. Mean ocean barotropic velocity for the REF (a) and nFST (b) simulations, average over the 1995-2014 period.

Figure A3, which shows the basal melt rate for the TIS and MUIS in WARM and WARM_noOce, indicates that the accelerated ASC decreases the basal melt rate in both cavities.

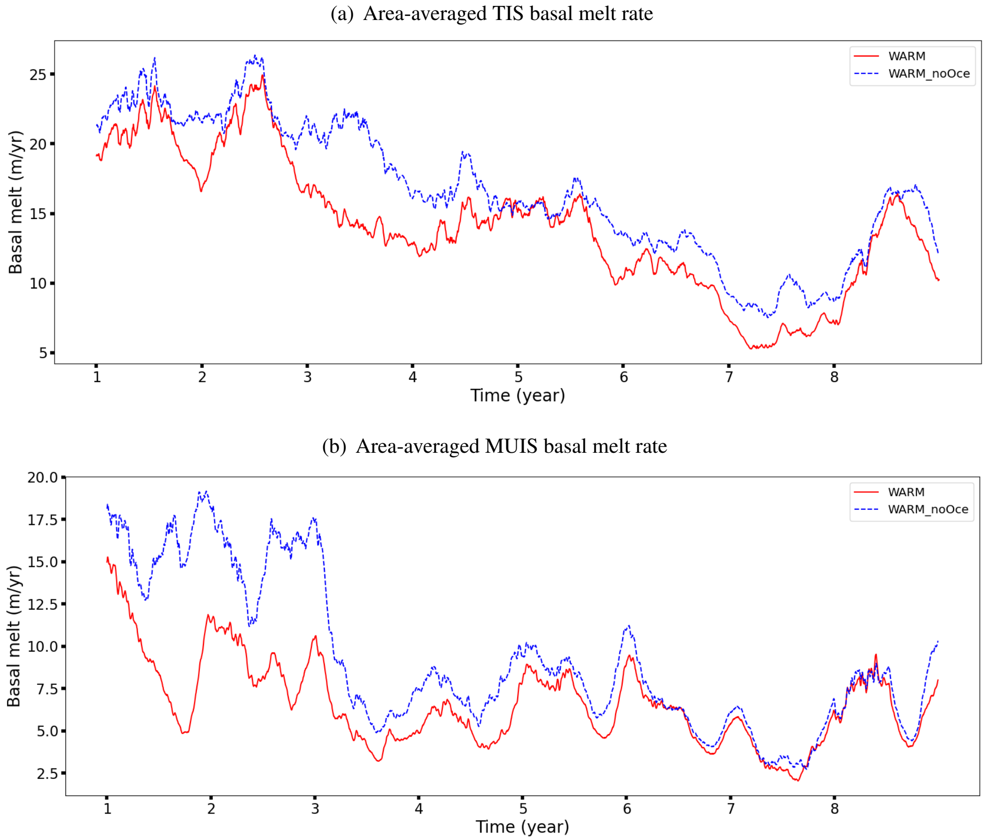

Figure A3. Time series of the area-averaged TIS (a) and MUIS (b) basal melt rate from WARM (red) and WARM_noOce (dotted blue) for the first 8 years of simulations.

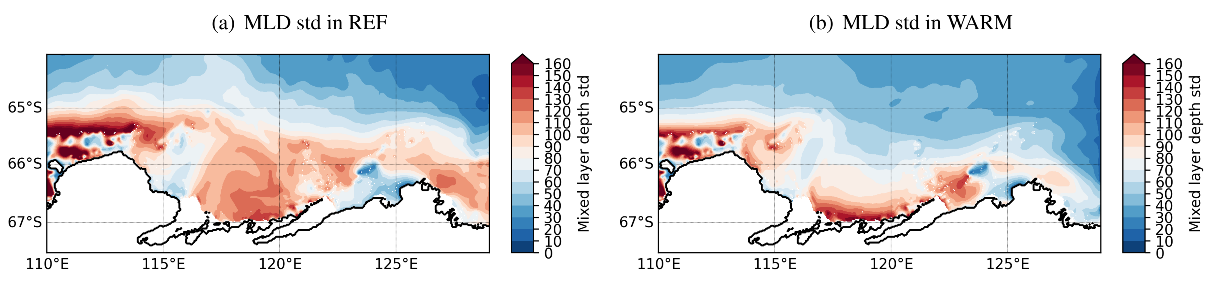

Figure A4. Standard deviation of the mixed layer depth for both REF (a) and WARM (b).

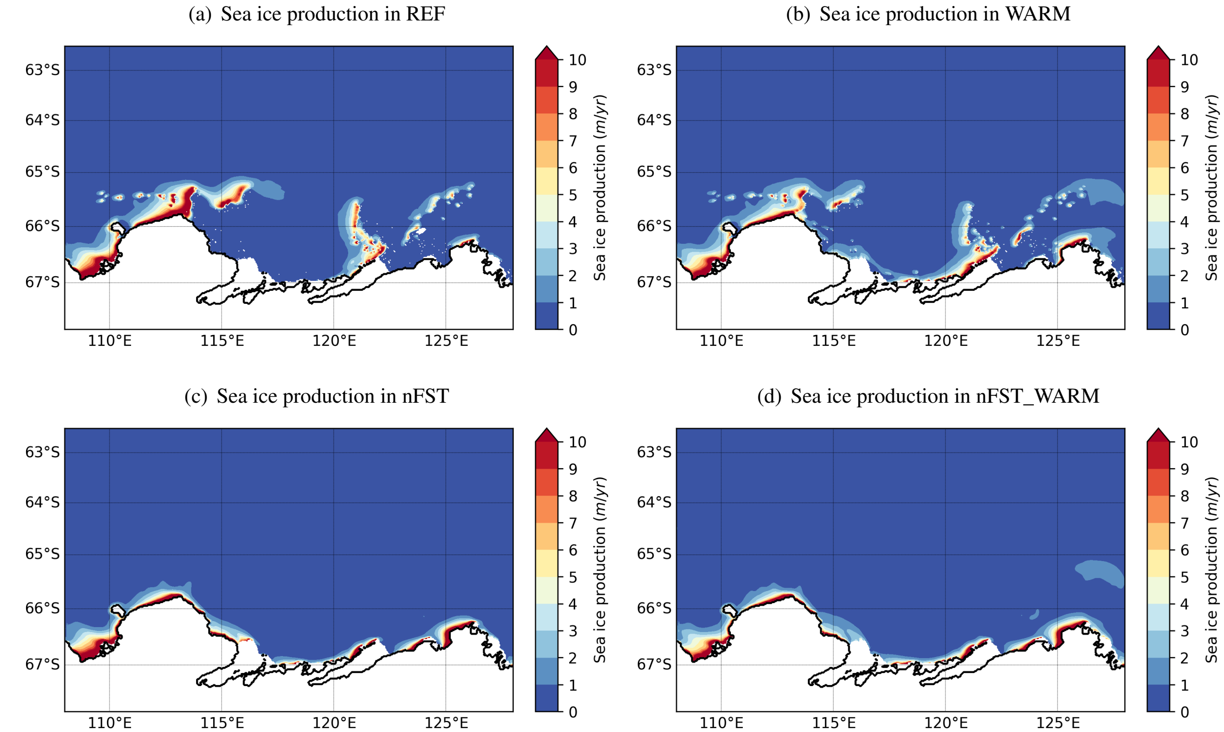

Figure A5. Mean sea ice production for REF (a), WARM (b), nFST (c) and nFST_WARM (d), all averaged over the 20 years of simulation.

Author contributions. GVA designed the science plan with TF and HG, ran the simulations, produced the figures, analysed the results and wrote the manuscript based on insights from all co-authors. EMC provided the EC–Earth3 dataset.

Competing interests. The authors declare that they have no known competing financial interests or personal relationships that could have appeared to influence the work reported in this paper.

Acknowledgements. This project (EOS O0100718F) has received funding from the FWO, Belgium and F.R.S.-FNRS, Belgium under the Excellence of Science (EOS) programme. HG is research director with the F.R.S-FNRS (Belgium). Computational resources have been provided by the supercomputing facilities of the Université catholique de Louvain (CISM/UCL) and the Consortium des Equipements de Calcul Intensif en Fédération Wallonie Bruxelles (CECI) funded by the Fond de la Recherche Scientifique de Belgique, Belgium (F.R.S.-FNRS) under convention 2.5020.11. The present research benefited from computational resources made available on the Tier-1 supercomputer of the Fédération Wallonie-Bruxelles, infrastructure funded by the Walloon Region under the grant agreement n1117545.

References

Adcroft, A., Hill, C., and Marshall, J.: Representation of Topography by Shaved Cells in a Height Coordinate Ocean Model, Mon. Weather Rev., 125, 2293 – 2315, https://doi.org/10.1175/1520-0493(1997)125<2293:ROTBSC>2.0.CO;2, 1997.

Aitken, A. R. A., Roberts, J. L., Ommen, T. D. v., Young, D. A., Golledge, N. R., Greenbaum, J. S., Blankenship, D. D., and Siegert, M. J.: Repeated large-scale retreat and advance of Totten Glacier indicated by inland bed erosion, Nature, 533, 385–389, https://doi.org/10.1038/nature17447, 2016.

Bitz, C. M., Holland, M. M., Weaver, A. J., and Eby, M.: Simulating the ice-thickness distribution in a coupled climate model, J. Geophys. Res. Oceans, 106, 2441–2463, https://doi.org/10.1029/1999JC000113, 2001.

Bougeault, P. and Lacarrere, P.: Parameterization of Orography-Induced Turbulence in a Mesobeta–Scale Model, Monthly Weather Review, 117, 1872–1890, https://doi.org/10.1175/1520-0493(1989)117<1872:POOITI>2.0.CO;2, 1989.

Carrère, L., Lyard, F., Cancet, M., Guillot, A., and Roblou, L.: A new global tidal model taking taking advantage of nearly 20 years of altimetry., Proceedings of meeting "20 Years of Altimerty", https://ui.adsabs.harvard.edu/abs/2013ESASP.710E..13C/abstract, 2012.

Dansereau, V., Heimbach, P., and Losch, M.: Simulation of subice shelf melt rates in a general circulation model: Velocity-dependent transfer and the role of friction, J. Geophys. Res. Oceans, 119, 1765–1790, https://doi.org/10.1002/2013JC008846, 2014.

Döscher, R., Acosta, M., Alessandri, A., Anthoni, P., Arneth, A., Arsouze, T., Bergmann, T., Bernadello, R., Bousetta, S., Caron, L.-P., Carver, G., Castrillo, M., Catalano, F., Cvijanovic, I., Davini, P., Dekker, E., Doblas-Reyes, F. J., Docquier, D., Echevarria, P., Fladrich, U., Fuentes-Franco, R., Gröger, M., v. Hardenberg, J., Hieronymus, J., Karami, M. P., Keskinen, J.-P., Koenigk, T., Makkonen, R., Massonnet, F., Ménégoz, M., Miller, P. A., Moreno-Chamarro, E., Nieradzik, L., van Noije, T., Nolan, P., O'Donnell, D., Ollinaho, P., van den Oord, G., Ortega, P., Prims, O. T., Ramos, A., Reerink, T., Rousset, C., Ruprich-Robert, Y., Le Sager, P., Schmith, T., Schrödner, R., Serva, F., Sicardi, V., Sloth Madsen, M., Smith, B., Tian, T., Tourigny, E., Uotila, P., Vancoppenolle, M., Wang, S., Wårlind, D., Willén, U., Wyser, K., Yang, S., Yepes-Arbós, X., and Zhang, Q.: The EC-Earth3 Earth System Model for the Climate Model Intercomparison Project 6, Geoscientific Model Development Discussions, 2021, 1–90, https://doi.org/10.5194/gmd-2020-446, 2021.

Engedahl, H.: Use of the flow relaxation scheme in a three-dimensional baroclinic ocean model with realistic topography, Tellus A: Dynamic Meteorology and Oceanography, 47, 365–382, https://doi.org/10.3402/tellusa.v47i3.11523, 1995.

Eyring, V., Bony, S., Meehl, G. A., Senior, C. A., Stevens, B., Stouffer, R. J., and Taylor, K. E.: Overview of the Coupled Model Intercomparison Project Phase 6 (CMIP6) experimental design and organization, Geoscientific Model Development, 9, 1937–1958, https://doi.org/10.5194/gmd-9-1937-2016, 2016.

Flather, R. A.: A Storm Surge Prediction Model for the Northern Bay of Bengal with Application to the Cyclone Disaster in April 1991, J. Phys. Oceanogr., 24, 172–190, https://doi.org/10.1175/1520-0485(1994)024<0172:ASSPMF>2.0.CO;2, 1994.

Fraser, A. D., Massom, R. A., Michael, K. J., Galton-Fenzi, B. K., and Lieser, J. L.: East Antarctic Landfast Sea Ice Distribution and Variability, 2000–08, J. Climate, 25, 1137–1156, https://doi.org/10.1175/JCLI-D-10-05032.1, 2012.

Fraser, A. D., Massom, R. A., Ohshima, K. I., Willmes, S., Kappes, P. J., Cartwright, J., and Porter-Smith, R.: High-resolution mapping of circum-Antarctic landfast sea ice distribution, 2000–2018, Earth Syst. Sci. Data, 12, 2987–2999, https://doi.org/10.5194/essd-12-2987-2020, 2020.

Gaspar, P., Grégoris, Y., and Lefevre, J.-M.: A simple eddy kinetic energy model for simulations of the oceanic vertical mixing: Tests at station Papa and long-term upper ocean study site, J. Geophys. Res. Oceans, 95, 16 179–16 193, https://doi.org/10.1029/JC095iC09p16179, 1990.

Greenbaum, J. S., Blankenship, D. D., Young, D. A., Richter, T. G., Roberts, J. L., Aitken, A. R. A., Legresy, B., Schroeder, D. M., Warner, R. C., van Ommen, T. D., and Siegert, M. J.: Ocean access to a cavity beneath Totten Glacier in East Antarctica, Nature Geoscience, 8, 294–298, https://doi.org/10.1038/ngeo2388, 2015.

Greene, C. A., Young, D. A., Gwyther, D. E., Galton-Fenzi, B. K., and Blankenship, D. D.: Seasonal dynamics of Totten Ice Shelf controlled by sea ice buttressing, The Cryosphere, 12, 2869 – 2882, https://doi.org/10.5194/tc-12-2869-2018, 2018.

Hellmer, H. H., Kauker, F., Timmermann, R., Determann, J., and Rae, J.: Twenty-first-century warming of a large Antarctic ice-shelf cavity by a redirected coastal current, Nature, 485, 225–228, https://doi.org/10.1038/nature11064, 2012.

Hersbach, H., Bell, B., Berrisford, P., Hirahara, S., Horányi, A., Muñoz-Sabater, J., Nicolas, J., Peubey, C., Radu, R., Schepers, D., Simmons, A., Soci, C., Abdalla, S., Abellan, X., Balsamo, G., Bechtold, P., Biavati, G., Bidlot, J., Bonavita, M., De Chiara, G., Dahlgren, P., Dee, D., Diamantakis, M., Dragani, R., Flemming, J., Forbes, R., Fuentes, M., Geer, A., Haimberger, L., Healy, S., Hogan, R. J., Hólm, E., Janisková, M., Keeley, S., Laloyaux, P., Lopez, P., Lupu, C., Radnoti, G., de Rosnay, P., Rozum, I., Vamborg, F., Villaume, S., and Thépaut, J.-N.: The ERA5 global reanalysis, Q. J. R. Meteorol. Soc., 146, 1999–2049, https://doi.org/10.1002/qj.3803, 2020.

Huot, P.-V., Fichefet, T., Jourdain, N. C., Mathiot, P., Rousset, C., Kittel, C., and Fettweis, X.: Influence of ocean tides and ice shelves on ocean–ice interactions and dense shelf water formation in the D'Urville Sea, Antarctica, Ocean Model., 162, 101 794, https://doi.org/https://doi.org/10.1016/j.ocemod.2021.101794, 2021.

IOC: The International thermodynamic equation of seawater: calculation and use of thermodynamic properties, Tech. rep., UNESCO, https://unesdoc.unesco.org/ark:/48223/pf0000188170, intergovernmental Oceanographic Commission, 2010.

Jacobs, S. S.: On the nature and significance of the Antarctic Slope Front, Marine Chemistry, 35, 9–24, https://doi.org/https://doi.org/10.1016/S0304-4203(09)90005-6, biochemistry and circulation of water masses in the Southern Ocean, 1991.

Jenkins, A.: A one-dimensional model of ice shelf-ocean interaction, J. Geophys. Res., 96, 20 671–20 677, https://doi.org/10.1029/91JC01842, 1991.

Jezek, K. C., Curlander, J. C., Carsey, F., Wales, C., and Barry, R. G.: RAMP AMM-1 SAR Image Mosaic of Antarctica, Version 2. [Indicate subset used], Boulder, Colorado USA. NASA National Snow and Ice Data Center Distributed Active Archive Center, https://doi.org/10.5067/8AF4ZRPULS4H, 2013.

Jourdain, N. C., Mathiot, P., Merino, N., Durand, G., Le Sommer, J., Spence, P., Dutrieux, P., and Madec, G.: Ocean circulation and sea-ice thinning induced by melting ice shelves in the Amundsen Sea, J. Geophys. Res. Oceans, 122, 2550–2573, https://doi.org/10.1002/2016JC012509, 2017.

Jourdain, N. C., Molines, J.-M., Le Sommer, J., Mathiot, P., Chanut, J., de Lavergne, C., and Madec, G.: Simulating or prescribing the influence of tides on the Amundsen Sea ice shelves, Ocean Model., 133, 44 – 55, https://doi.org/10.1016/j.ocemod.2018.11.001, 2019.

Khazendar, A., Schodlok, M., Fenty, I., Ligtenberg, S., Rignot, E., and van den Broeke, M.: Observed thinning of Totten Glacier is linked to coastal polynya variability, Nat. Commun., 4, https://doi.org/10.1038/ncomms3857, 2013.

Large, W. and Yeager, S.: Diurnal to decadal global forcing for ocean and sea-ice models: the data sets and flux climatologie, UCAR, https://doi.org/10.5065/D6KK98Q6, 2004.

Lemieux, J.-F., Dupont, F., Blain, P., Roy, F., Smith, G. C., and Flato, G. M.: Improving the simulation of landfast ice by combining tensile strength and a parameterization for grounded ridges, J. Geophys. Res. Oceans, 121, 7354–7368, https://doi.org/10.1002/2016JC012006, 2016.

Lockwood, J. W., Dufour, C. O., Griffies, S. M., and Winton, M.: On the Role of the Antarctic Slope Front on the Occurrence of the Weddell Sea Polynya under Climate Change, Journal of Climate, 34, 2529 – 2548, https://doi.org/10.1175/JCLI-D-20-0069.1, 2021.

Losch, M.: Modeling ice shelf cavities in a z coordinate ocean general circulation model, J. Geophys. Res. Oceans, 113, https://doi.org/10.1029/2007JC004368, 2008.

Madec, G.: NEMO ocean engine, Note du Pole de modelisation, Institut Pierre-Simon Laplace (IPSL), France, No 27, ISSN No 1288-1619, 2008.

Madec, G., Delecluse, P., Imbard, M., and Levy, C.: 1 Ocean General Circulation Model reference manual, 1998.

Maraldi, C., Chanut, J., Levier, B., Ayoub, N., De Mey, P., Reffray, G., Lyard, F., Cailleau, S., Drévillon, M., Fanjul, E. A., Sotillo, M. G., Marsaleix, P., the Mercator Research, and Team, D.: NEMO on the shelf: assessment of the Iberiandash;Biscayndash;Ireland configuration, Ocean Sci., 9, 745–771, https://doi.org/10.5194/os-9-745-2013, 2013.

Massom, R. A., Hill, K. L., Lytle, V. I., Worby, A. P., Paget, M., and Allison, I.: Effects of regional fast-ice and iceberg distributions on the behaviour of the Mertz Glacier polynya, East Antarctica, Ann. Glaciol., 33, 391–398, https://doi.org/10.3189/172756401781818518, 2001.

Massonnet, F., Goosse, H., Fichefet, T., and Counillon, F.: Calibration of sea ice dynamic parameters in an ocean-sea ice model using an ensemble Kalman filter, Journal of Geophysical Research: Oceans, 119, 4168–4184, https://doi.org/10.1002/2013JC009705, 2014.

Mathiot, P., Goosse, H., Fichefet, T., Barnier, B., and Gallée, H.: Modelling the seasonal variability of the Antarctic Slope Current, Ocean Science, 7, 455–470, https://doi.org/10.5194/os-7-455-2011, 2011.

Mathiot, P., Jenkins, A., Harris, C., and Madec, G.: Explicit representation and parametrised impacts of under ice shelf seas in the z^* coordinate ocean model NEMO 3.6, Geosci. Model Dev., 10, 2849–2874, https://doi.org/10.5194/gmd-10-2849-2017, 2017.

Moorman, R., Morrison, A. K., and Hogg, A. M.: Thermal Responses to Antarctic Ice Shelf Melt in an Eddy-Rich Global Ocean–Sea Ice Model, Journal of Climate, 33, 6599 – 6620, https://doi.org/10.1175/JCLI-D-19-0846.1, 2020.

Morlighem, M., Rignot, E., Binder, T., Blankenship, D., Drews, R., Eagles, G., Eisen, O., Forsberg, R., Fretwell, P., Goel, V., Greenbaum, J., Gudmundsson, G., Guo, J., Helm, V., Hofstede, C., Howat, I., Humbert, A., Jokat, W., and Young, D.: Deep glacial troughs and stabilizing ridges unveiled beneath the margins of the Antarctic ice sheet, Nat. Geosci., 13, 1–6, https://doi.org/10.1038/s41561-019-0510-8, 2020.

Nakayama, Y., Greene, C. A., Paolo, F. S., Mensah, V., Zhang, H., Kashiwase, H., Simizu, D., Greenbaum, J. S., Blankenship, D. D., Abe-Ouchi, A., and Aoki, S.: Antarctic Slope Current Modulates Ocean Heat Intrusions Towards Totten Glacier, Geophysical Research Letters, 48, e2021GL094 149, https://doi.org/10.1029/2021GL094149, 2021.

Naughten, K. A., Meissner, K. J., Galton-Fenzi, B. K., England, M. H., Timmermann, R., and Hellmer, H. H.: Future Projections of Antarctic Ice Shelf Melting Based on CMIP5 Scenarios, Journal of Climate, 31, 5243 – 5261, https://doi.org/10.1175/JCLI-D-17-0854.1, 2018.

Nihashi, S. and Ohshima, K. I.: Circumpolar Mapping of Antarctic Coastal Polynyas and Landfast Sea Ice: Relationship and Variability, J. Climate, 28, 3650–3670, https://doi.org/10.1175/JCLI-D-14-00369.1, 2015.

Paolo, F. S., Fricker, H. A., and Padman, L.: Volume loss from Antarctic ice shelves is accelerating, Science, 348, 327–331, https://doi.org/10.1126/science.aaa0940, 2015.

Pelle, T., Morlighem, M., Nakayama, Y., and Seroussi, H.: Widespread Grounding Line Retreat of Totten Glacier, East Antarctica, Over the 21st Century, Geophys. Res. Lett., 48, e2021GL093 213, https://doi.org/10.1029/2021GL093213, 2021.

Pelletier, C., Fichefet, T., Goosse, H., Haubner, K., Helsen, S., Huot, P.-V., Kittel, C., Klein, F., Le clec'h, S., van Lipzig, N. P. M., Marchi, S., Massonnet, F., Mathiot, P., Moravveji, E., Moreno-Chamarro, E., Ortega, P., Pattyn, F., Souverijns, N., Van Achter, G., Vanden Broucke, S., Vanhulle, A., Verfaillie, D., and Zipf, L.: PARASO, a circum-Antarctic fully-coupled ice-sheet - ocean - sea-ice - atmosphere - land model involving f.ETISh1.7, NEMO3.6, LIM3.6, COSMO5.0 and CLM4.5, Geosci. Model Dev., 15, 553–594, https://doi.org/10.5194/gmd-2021-315, 2022.

Pellichero, V., Sallée, J.-B., Chapman, C. C., and Downes, S. M.: The southern ocean meridional overturning in the sea-ice sector is driven by freshwater fluxes, Nat. Commun., 9, https://doi.org/10.1038/s41467-018-04101-2, 2018.

Rignot, E., Jacobs, S., Mouginot, J., and Scheuchl, B.: Ice-Shelf Melting Around Antarctica, Science, 341, 266–270, https://doi.org/10.1126/science.1235798, 2013.

Rintoul, S. R., Silvano, A., Pena-Molino, B., van Wijk, E., Rosenberg, M., Greenbaum, J. S., and Blankenship, D. D.: Ocean heat drives rapid basal melt of the Totten Ice Shelf, Sci. Adv., 2, https://doi.org/10.1126/sciadv.1601610, 2016.

Roberts, J. L., Warner, R. C., Young, D., Wright, A., van Ommen, T. D., Blankenship, D. D., Siegert, M., Young, N. W., Tabacco, I. E., Forieri, A., Passerini, A., Zirizzotti, A., and Frezzotti, M.: Refined broad-scale sub-glacial morphology of Aurora Subglacial Basin, East Antarctica derived by an ice-dynamics-based interpolation scheme, The Cryosphere, 5, 551–560, https://doi.org/10.5194/tc-5-551-2011, 2011.

Roquet, F., Williams, G., Hindell, M. A., Harcourt, R., McMahon, C., Guinet, C., Charrassin, J.-B., Reverdin, G., Boehme, L., Lovell, P., and Fedak, M.: A Southern Indian Ocean database of hydrographic profiles obtained with instrumented elephant seals, Scientific Data, 1, https://doi.org/10.1038/sdata.2014.28, 2014.

Rousset, C., Vancoppenolle, M., Madec, G., Fichefet, T., Flavoni, S., Barthélemy, A., Benshila, R., Chanut, J., Levy, C., Masson, S., and Vivier, F.: The Louvain-La-Neuve sea ice model LIM3.6: global and regional capabilities, Geosci. Model Dev., 8, 2991–3005, https://doi.org/10.5194/gmd-8-2991-2015, 2015.

Stewart, A. L., Klocker, A., and Menemenlis, D.: Circum-Antarctic Shoreward Heat Transport Derived From an Eddy- and Tide-Resolving Simulation, Geophysical Research Letters, 45, 834–845, https://doi.org/10.1002/2017GL075677, 2018.

Thompson, A. F., Stewart, A. L., Spence, P., and Heywood, K. J.: The Antarctic Slope Current in a Changing Climate, Reviews of Geophysics, 56, 741–770, https://doi.org/10.1029/2018RG000624, 2018.

Timmermann, R. and Goeller, S.: Response to Filchner–Ronne Ice Shelf cavity warming in a coupled ocean–ice sheet model – Part 1: The ocean perspective, Ocean Science, 13, 765–776, https://doi.org/10.5194/os-13-765-2017, 2017.

Van Achter, G., Fichefet, T., Goosse, H., Pelletier, C., Sterlin, J., Huot, P.-V., Lemieux, J.-F., Fraser, A. D., Haubner, K., and Porter-Smith, R.: Modelling landfast sea ice and its influence on ocean–ice interactions in the area of the Totten Glacier, East Antarctica, Ocean Model., 169, 101 920, https://doi.org/10.1016/j.ocemod.2021.101920, 2022.

Vancoppenolle, M., Fichefet, T., Goosse, H., Bouillon, S., Madec, G., and Maqueda, M.: Simulating the mass balance and salinity of Arctic and Antarctic sea ice. 1. Model description and validation, Ocean Model., 27, 33 – 53, https://doi.org/10.1016/j.ocemod.2008.10.005, 2009.

Whitworth, T., Orsi, A. H., Kim, S.-J., Nowlin Jr., W. D., and Locarnini, R. A.: Water Masses and Mixing Near the Antarctic Slope Front, pp. 1–27, American Geophysical Union (AGU), https://doi.org/10.1029/AR075p0001, 1985.

WMO: WMO sea-ice nomenclature. Terminology, codes and illustrated glossary, Tech. Rep., 259, 1970.